A preliminary study of crustal structure in Taiwan region using receiver function analysis

Kwang-Hee Kim,[1] Jer-Ming Chiu,[1] Honn Kao,[2] Qiyuan Liu[3] and Yih-Hsiung Yeh[2]

[1] *Center for Earthquake Research and Information, The University of Memphis, Memphis,* TN 38152, *USA. E-mail: chiu@ceri.memphis.edu*
[2] *Institute of Earth Sciences, Academia Sinica,* PO Box 1-55, *Nankang, Taipei,* 115, *Taiwan*
[3] *Institute of Geology, Chinese Seismological Bureau, Beijing,* 100029, *China*

SUMMARY

Selected teleseismic data observed at temporary and permanent broad-band stations have been analysed using the receiver function method in order to investigate the very complex crustal structure in Taiwan region. Very significant azimuthal variations of radial and transverse receiver function responses from broad-band stations could be attributed to, among other things, the sampling of incoming seismic waves across the nearby subduction zone, a subsurface dipping interface, or a localized anisotropic region. A mid-crust discontinuity, interpreted as the Conrad discontinuity, can be identified at 18–20 km depth beneath TATO and TPUB stations in the Western Foothills, but is absent beneath the two nearby stations SSLB and TDCB in the Central Mountain Range. The separation of upper and lower crust beneath the Western Foothills and the steady increase in crustal velocity as a function of depth across the entire thicker crust beneath the Central Mountain Range suggest that the tectonic evolution of the crust may be significantly different for these two adjacent regions. Although a 'thin-skinned' model may be associated with the tectonic evolution of the upper crust of the Western Foothills and Western Coastal Plain, a 'thick-skinned' or 'lithospheric deformation' model can probably be applied to explain the crustal evolution of the Central Mountain Range. A trend of crustal thinning from east (50–52 km) to west (28–32 km) is in very good agreement with the results from two east–west-trending deep seismic profiles obtained using airgun sources. The thinner crust (20–30 km) beneath TWB1 station in northeastern Taiwan can be associated with the high-heat-flow backarc opening at the western terminus of the Okinawa trough behind the subduction of the Philippine Sea plate. The relatively simple crustal structure beneath KMNB station, offshore southeastern China, depicts typical continental crust, with the Moho depth at 28–32 km. An apparent offset of the thickest Moho beneath NACB station from the topographic high in the central Central Mountain Range suggests that the Taiwan orogeny has probably not reached its isostatic status.

Key words: broad band, crustal structure, Moho, receiver function.

GJI Seismology

INTRODUCTION

The island of Taiwan is located along the Eurasian and the Philippine Sea plate boundary. A mix of active subduction and collision between the two plates has contributed to the active mountain building processes and tectonic evolution around the Taiwan region. In northern Taiwan, the Philippine Sea plate has been subducting beneath the Eurasian plate in a NW direction along the Ryukyu arc, while in southern Taiwan, the South China Sea plate has been subducting eastwards beneath the Luzon arc of the Philippine Sea plate (Fig. 1). Between the two subduction zones, the Eurasian plate and the Philippine Sea plate collide in central eastern Taiwan along a north–south-trending suture zone, known as the Longitudinal Valley. As a consequence of plate collision, actively uplifted and highly meta-

morphosed mountain ranges formed, including the Central Mountain Range to the west of the suture zone on the Eurasian plate and the Coastal Range to the east of the suture zone on the Philippine Sea plate. As shown in the summary of major tectonic units in Taiwan region (Fig. 2), the continental margin part of Taiwan consists of four NNE–SSW-trending structural belts based on rock type and degree of deformation. From west to east, the Coastal Plain, the Western Foothills, the Western Central Range, and the Eastern Central Range are separated by faults or structural discontinuities (Ho 1988). The orogeny in Taiwan region is very young, commencing about 4 million years ago, and is still very active. Owing to the oblique collision of the Luzon arc with the continental margin, the younger collision zone in Taiwan is extending southwards, i.e. the collision is more advanced along the northern
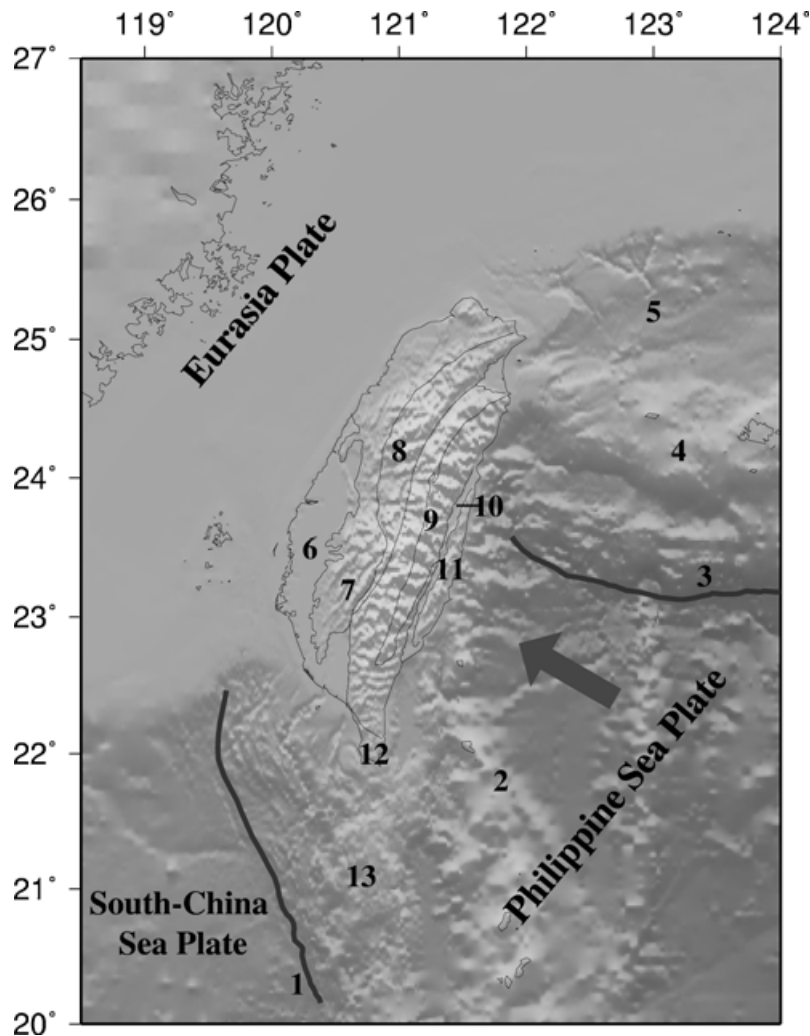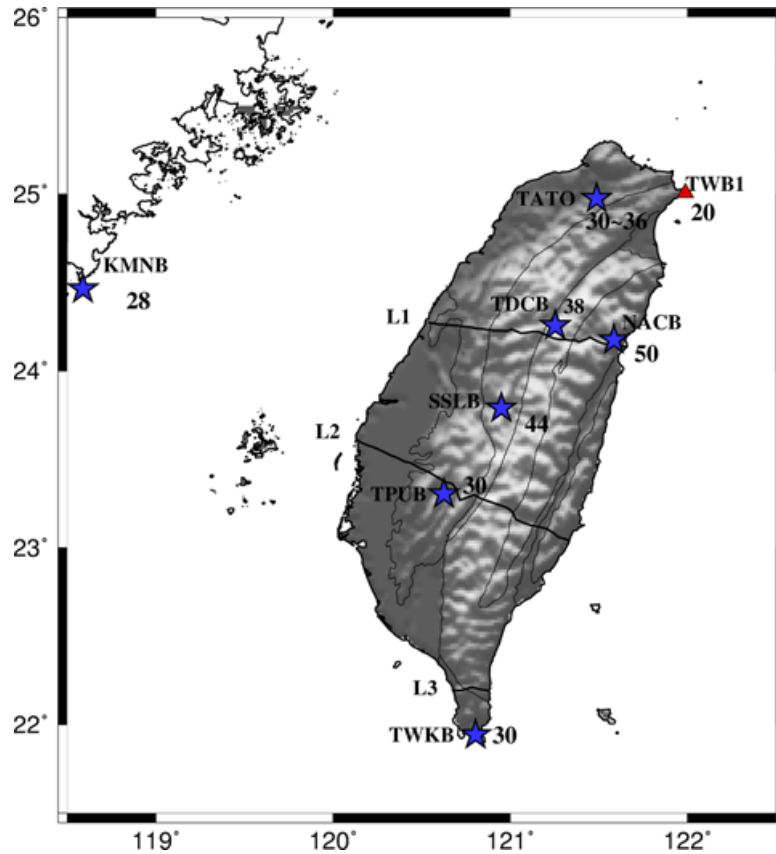
Figure 1. Tectonic map around Taiwan region showing that the regional tectonic process is governed by the convergence of Philippine Sea and Eurasian plates. The convergence rate between the two plates is among the highest in the world (8.3 cm yr^{-1}), so Taiwan region is characterized by one of the world's youngest and the most vigorous mountain-building processes. The major tectonic units associated with the active subduction and collision in Taiwan region include (1) Luzon trench, (2) Luzon arc, (3) Ryukyu trench, (4) Ryukyu arc, (5) Okinawa trough, (6) Western Coastal Plain, (7) Western Foothills, (8) Western Central Mountain Range, (9) Eastern Central Mountain Range, (10) Longitudinal Valley, (11) Coastal Range, (12) Hengchun Peninsula, and (13) Hengchun Ridge.

Longitudinal Valley and is in its initial stage in southeastern Taiwan (Teng 1990).

Several models have been proposed to interpret the orogeny in Taiwan. A 'thin-skinned' deformation model was proposed by Suppe (1976, 1980, 1981, 1984, 1987), based on sedimentology and stratigraphy in the Western Foothills under the assumptions of initially flat-lying sedimentary units over a continuous basal decollment, uniaxial and continuous east–west compression, and a limited amount of basement involvement. Suppe's model considered the development of the Taiwan orogeny as resembling the 'thin-skinned' growth of a wedge of soil pushed in front by a moving bulldozer over an underlying basal detachment. However, seismicity and focal mechanism studies from local seismic networks suggest that significant deformation is taking place in the mid- to lower crust at a level that is far below what the 'thin-skinned' tectonics hypothesis predicts. Therefore, an alternative 'lithospheric collision' model has been proposed by Wu *et al.* (1997) which suggests that deformation associated with the entire thickness of lithosphere must be involved in the Taiwan orogeny, based on the distribution of earthquake hypocentres.

Several crustal structural models for Taiwan region have recently been determined. From a 3-D tomographic inversion of regional seismic network data, Rau & Wu (1995) showed that crustal thickness varies significantly across the entire island of Taiwan. Using a similar database from a regional seismic network but slightly different selection criteria, Ma *et al.* (1996) estimated a crustal thickness of 30–35 km for Taiwan island on the Eurasian plate and of 15–20 km on the Philippine Sea plate. However, crustal structure images obtained by Rau & Wu (1995) and by Ma *et al.* (1996) are, in general, not consistent with each other. A recent report by Pujol (2000) indicated that the application of a well-established 3-D tomographic inversion algorithm to excellent data with excellent station coverage will definitely produce 3-D tomographic images. However, there is no guarantee that a realistic result will emerge if there are significant lateral velocity variations, or if the initial velocity model for inversion is too far from the real model. The difference in 3-D structural results between Rau & Wu (1995) and Ma *et al.* (1996) may be due to different selection criteria from a similar database, or to different initial models, or to different approaches in inversion, or to all of the above.

Figure 2. Topographic map of Taiwan region showing the major tectonic units that include, from west to east, I Coastal Plain, II Western Foothills, III Western Central Mountain Range, IIIa Hsuehshan Range, IIIb Backbone Range Belt, IV Eastern Central Range, V Eastern Coastal Range, VI Longitudinal Valley (site of collisional suture). Locations of BATS stations are shown by solid stars. Locations of temporary PASSCAL stations deployed in 1995 are shown by solid triangles. The three onshore/offshore wide-angle deep seismic profiles are shown as L1, L2 and L3.
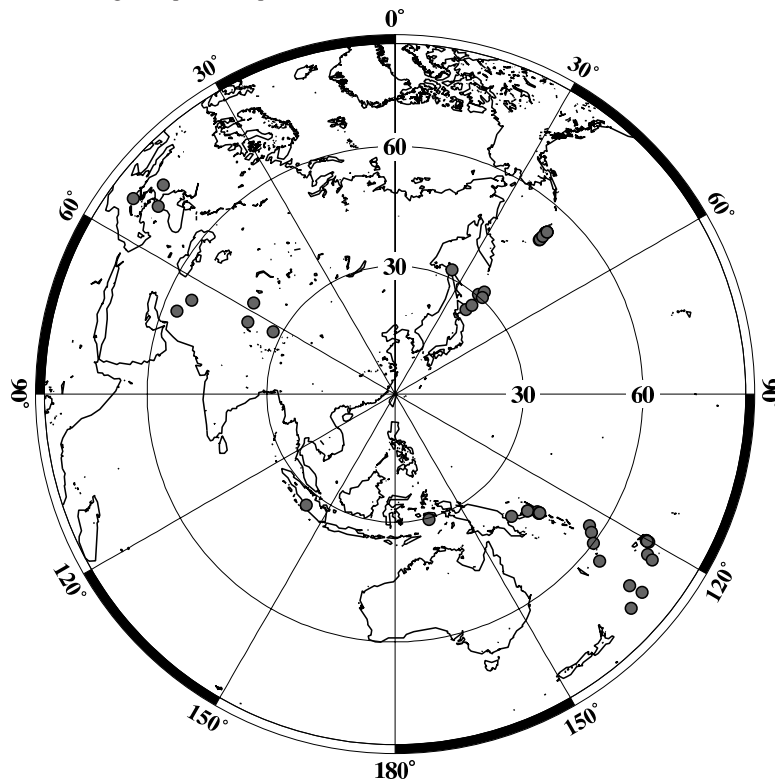
Figure 3. Map showing epicentres of the selected teleseismic events (solid circles) used in this study. Earthquakes are selected based on consideration of epicentral distance ($25° < \Delta < 100°$), magnitude (>6.5), and high signal-to-noise ratio on observed seismograms.

In a recent modelling of gravity data, Yen *et al.* (1998) revealed that the Moho depth is about 26 km beneath the Coastal Plain and the Western Foothills, 28 km beneath the Coastal Range in eastern Taiwan, and 33 km beneath the Central Range. Based on magnetotelluric observations, Chen *et al.* (1998) proposed that the Moho discontinuity is probably at a depth of 20–30 km beneath the central and southern Central Mountain Range. From the modelling and interpretation of deep seismic profiles using airgun sources, Yeh *et al.* (1998) and Shih *et al.* (1998) provided a first direct glimpse of the crustal structure and Moho configuration along the southern and central cross-island highways, respectively. Their models from seismic profiles include a thin crust of 10 km for the Philippine Sea plate, which increases to 50 km beneath the Central Mountain Range and decreases to 36 km beneath the Coastal Plain. However, the Moho depths along the east–west cross-section determined by Shih *et al.* (1998) are in general slightly shallower than those obtained by Yeh *et al.* (1998).

Thus, our current understanding of crustal and upper mantle structure in Taiwan region are jeopardized by the limited resolution of 3-D tomographic inversion (e.g. Rau & Wu 1995; Ma *et al.* 1996) and the non-uniqueness of gravity, seismic, and other data modelling (e.g. Yen *et al.* 1998; Chen *et al.* 1998; Yeh *et al.* 1998; Shih *et al.* 1998). Receiver function analysis of broad-band data can provide an independent assessment of crustal velocity structure variations in Taiwan region, although the broad-band stations in Taiwan region are sparsely distributed.

RECEIVER FUNCTION ANALYSIS

Since digital broad-band seismic data became available, the receiver function analysis method has had a significant impact on the study of the structure of the Earth's crust and upper mantle (e.g. Burdick & Langston 1977; Langston 1977, 1979, 1981; Owens *et al.* 1984, 1987; Ammon *et al.* 1990; Ammon 1991; Cassidy 1992; Liu *et al.* 1996, 1997, 1998). The basic idea of receiver function analysis is that subsurface structures beneath a seismic station can be retrieved from information in seismic wave trains, which usually contain seismic arrivals specifically associated with subsurface discontinuities. For example, the *P*-to-*S* wave conversion as well as the transmitted *P* wave from a discontinuity beneath a station are commonly observed from teleseismic events, and can be analysed to determine the depth and other elastic parameters of the discontinuity. In comparison with the method of direct forward modelling of the teleseismic *P* waveform for structure study, receiver function analysis has the advantage that the considerations of complicated earthquake-source and near-source reverberations can be avoided.

In the time domain, the displacement response $D(t)$ for a teleseismic *P* wave impinging under a stack of horizontal interfaces can be written as

$$D_V(t) = I(t) * S(t) * E_V(t),$$
$$D_R(t) = I(t) * S(t) * E_R(t),$$
$$D_T(t) = I(t) * S(t) * E_T(t), \qquad (1)$$
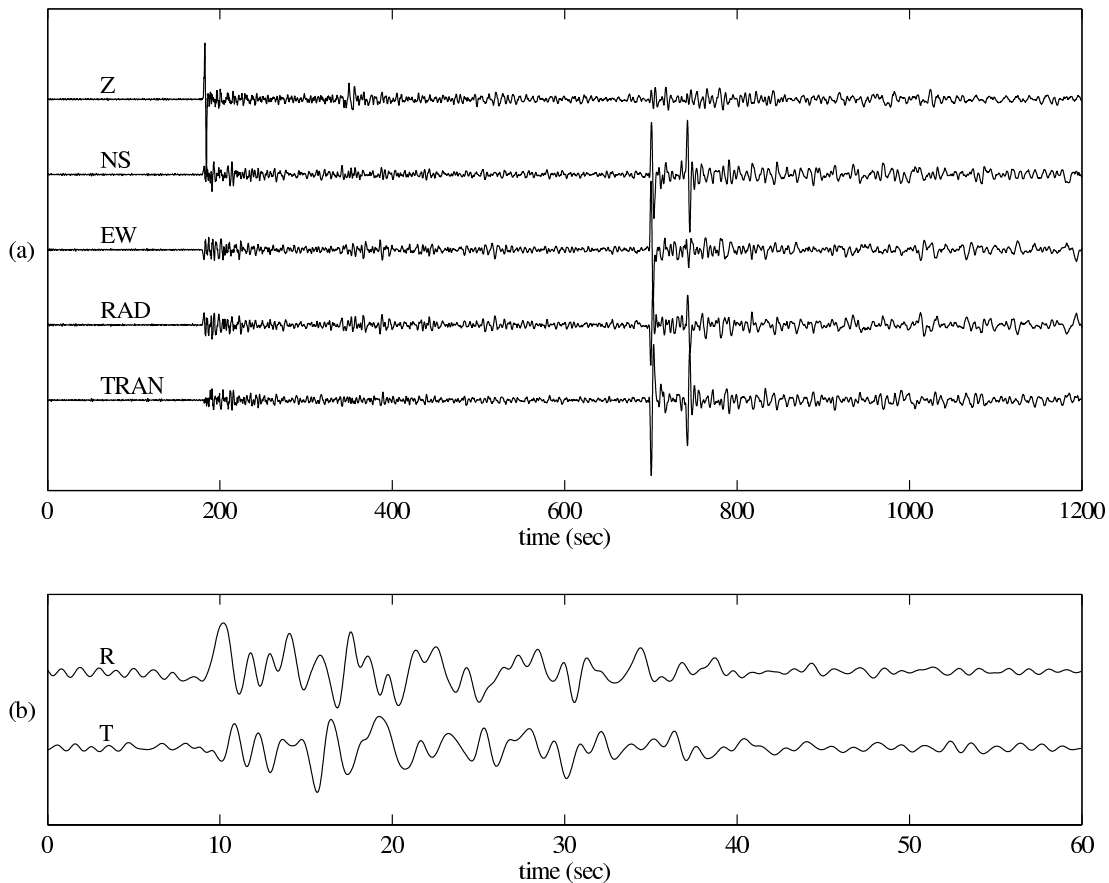
Figure 4. (a) A typical three-component teleseismic broad-band seismogram for a deep Fiji Island earthquake (573 km) recorded at station TATO (upper three traces); and the radial and transverse components after rotation (fourth and fifth traces). (b) Radial (R) and transverse (T) receiver responses after a source equalization (deconvolution) process.

where

$I(t)$: Impulse response of the recording instrument.
$S(t)$: Seismic source function.
$E(t)$: Impulse response of near-receiver Earth structure.
V, R, T : Vertical, radial and transverse, respectively.
$*$: Convolution operator.

Under the general assumption of isotropic material, horizontally layered subsurface structure, and vertically incident seismic waves, the receiver response from the incident P waves and the P-to-S (P_s) converted waves from near-receiver discontinuities should be polarized and restrained only in the radial and vertical planes. The transverse component of the receiver function is expected to be negligible. In many cases, however, significant seismic energy has been observed on the transverse component, which may be associated with dipping structure (e.g. Langston 1977; Zhang & Langston 1995; Chen & Liu 1999) and/or a subsurface anisotropic body (e.g. Baker *et al.* 1996; Peng & Humphreys 1997).

To isolate the receiver response from teleseismic P waveforms, a deconvolution technique, namely the 'source equalization' procedure (Langston 1979), has been applied to extract a function that depends almost purely on the subsurface structures just beneath the

Figure 5. Radial-component receiver functions for TATO station from earthquakes at different backazimuths (BAZ) and epicentral distances (DIST), both in degrees. Similar and slightly different receiver functions are apparent from events of similar and different azimuths, respectively. The first three traces of similar azimuths and similar receiver functions can be stacked (summed) to constitute a representative receiver function from the NE direction, as shown in the second trace from the bottom. The next 10 events within backazimuth ranges from 119.99° to 131.17° show similar receiver functions so they can be stacked to form a representative receiver function from the SE direction (bottom trace).

recording station:

$$E_{\mathrm{R}}(\omega) = \frac{D_{\mathrm{R}}(\omega)}{I(\omega)S(\omega)} \simeq \frac{D_{\mathrm{R}}(\omega)}{D_{\mathrm{V}}(\omega)},$$

$$E_{\mathrm{T}}(\omega) = \frac{D_{\mathrm{T}}(\omega)}{I(\omega)S(\omega)} \simeq \frac{D_{\mathrm{T}}(\omega)}{D_{\mathrm{V}}(\omega)}. \tag{2}$$
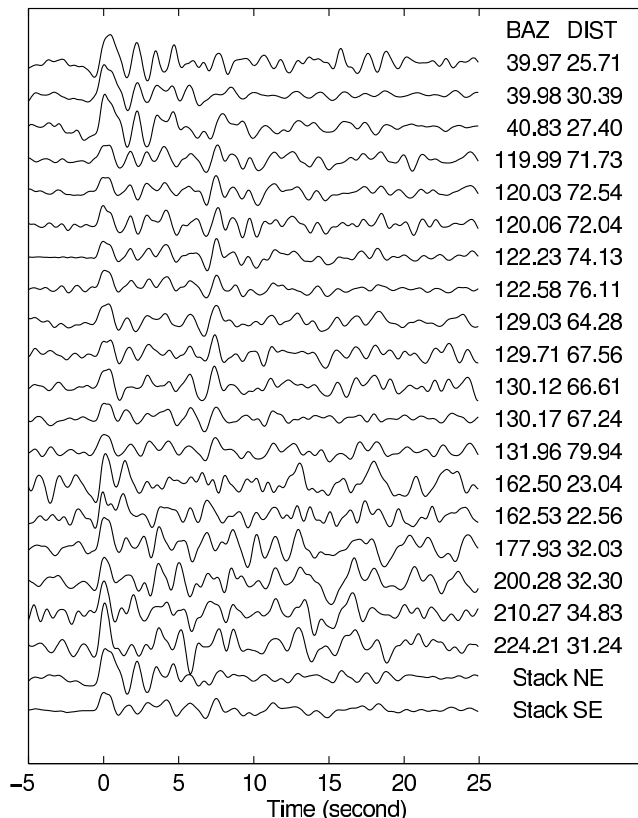
Vertical-component seismograms from teleseismic data of deep events are usually characterized by impulsive first arrivals followed by minor later arrivals. These observations of teleseismic events justify the assumption introduced here, namely $I(t) * S(t) \simeq D_{\mathrm{V}}(t)$ (Langston 1979). In practice, numerical problems may occur in spectral division when the denominator is very small. A water-level deconvolution method (Clayton & Wiggins 1976) was adopted by Langston (1979) to prevent unstable numerical calculation resulting from an extremely small denominator. This estimate after water-level deconvolution is then multiplied by the transform of a Gaussian function to simplify the resultant receiver function, and a low-pass filter is applied to remove any high-frequency noise that did not exist in the original recordings (Langston 1979). The Gaussian function is applied because of its simple shape, zero phase distortion, and minimal side-lobes.

After source equalization, a few receiver functions may be stacked to improve the signal-to-noise ratio and to determine a representative receiver function. By stacking receiver functions for events of similar azimuths, the random noise will be minimized and the coherent signals will be enhanced to improve the reliability of the representative receiver function beneath a station. Stacking of receiver functions is recommended under two circumstances: (1) stacking within a group of similar backazimuths if there is any dipping structure or a complex tectonic environment; and (2) stacking over all directions if there is no significant azimuthal variation of receiver functions, suggesting a nearly flat layer structure. Even though apparent differences in receiver functions are commonly found, stacking over different backazimuths to offer an average estimate of crustal structure is still justified. In an environment of dipping layers, a stacking of receiver functions is valid only for events whose differences in epicentral distance and backazimuth are less than 10° (Cassidy 1992).

MAXIMAL LIKELIHOOD ESTIMATION OF THE RECEIVER FUNCTION

A method developed by Liu *et al.* (1996, 1997) was used to estimate the complex spectrum ratio between the radial and vertical components of the receiver function from the broad-band teleseismic P waveforms. Their method is characterized by a stable deconvolution process based on the multichannel maximal likelihood deconvolution theory of Shumway & Der (1985) and by a non-linear inversion algorithm of the complex spectrum ratio of the receiver function based on the waveform inversion theory of Tarantola (1987).

Source equalization is valid only when the receiver structure is simple and smooth. When there are sharp discontinuities in the upper crust, or the focal depth of an event is shallow, the interaction of P waves with the surface or near-surface reflected or converted waves will become significant, so that the vertical-component receiver function can no longer be considered as a simple δ function in broad-band seismic observation (Langston 1979; Ammon 1991; Liu *et al.* 1996). In most cases, a water level is arbitrarily selected to stabilize the deconvolution process, which may affect the resolution as well as the signal-to-noise ratio of the receiver function. Since the amplitude spectrum of seismic waves usually decays faster at higher

frequencies, Liu *et al.* (1996) proposed selecting two water levels with different magnitudes during spectral division, one for lower- and the other for higher-frequency ranges, in order to achieve a stable deconvolution process.

Three-component receiver functions are assumed to be independent of each other. In the case where noise exists, the complex spectra of the three-component teleseismic *P* waves can be expressed as

$$Y_{lk}(\omega) = X_k(\omega)R_l(\omega) + N_{lk}(\omega), \qquad (3)$$

where $k = 1, 2, ..., n$ (*n* being the total number of events), and $l = 1, 2, 3$ for the vertical, north–south, and east–west components, respectively.

$Y(\omega)$ and $R(\omega)$ are the complex spectra of the teleseismic *P* waves and the receiver function beneath the station, respectively. $X_k(\omega)$ is defined as a function for the *k*th event consisting of the source time function, the impulsive response of the Earth except at the receiver area, and the instrument response. $N_{lk}(\omega)$ represents the noise related to the *l*th component for the *k*th event. By regarding the $X_k(\omega)$ function in eq. (3) as stochastic and the receiver function $R(\omega)$ as an invariant unknown, the invariant unknowns can be estimated by maximizing a frequency-domain approximation to the likelihood. A multi-channel maximum likelihood deconvolution (MMLD) algorithm proposed by Shumway & Der (1985) and adapted by Liu *et al.* (1996) has been applied in this study to estimate the source functions $X_k(\omega)$ and receiver functions $R_l(\omega)$ in eq. (3). The MMLD begins by initializing the receiver functions, noise levels, and signal-to-noise ratios. A simple delta function may be used as the initial receiver function in the first iteration. The noise level can be es-

timated from the background noise before the onset. The source factor and the variance of the source factor can thus be estimated. After the calculation of the mean receiver function, an updated signal spectrum and noise spectrum can be obtained. The updated noise spectrum and signal spectrum are used in the next iteration to calculate the source factor and variance of the source factor. The iteration continues until a minimum variance of the source factor $[X_k(\omega)]$ is achieved and the conditional maximal likelihood estimation of the receiver functions $[R_l(\omega)]$ is thus obtained. In this algorithm, the receiver function is estimated as a common factor for an array of events, and arbitrary selection of a water level is unnecessary by virtue of using the variance of the source factor. It can also be noted that the receiver function is derived from a linear model.

DATA

A broad-band seismic network (BATS, Broad-Band Array in Taiwan for Seismology) has been installed in Taiwan region by the Institute of Earth Sciences, Academia Sinica (IESAS). By 1997, the BATS broad-band network consists of 11 stations, including one Global Seismic Network (GSN) station, TATO, in northern Taiwan (Fig. 2). Selected data from nine BATS stations are used in this study. In addition, selected data from a temporary deployment of 12 PASSCAL (Program for the Array Seismic Studies of the Continental Lithosphere) broad-band stations in 1995 are available (Fig. 2). Since most temporary broad-band stations were located in coastal regions and the period of deployment was
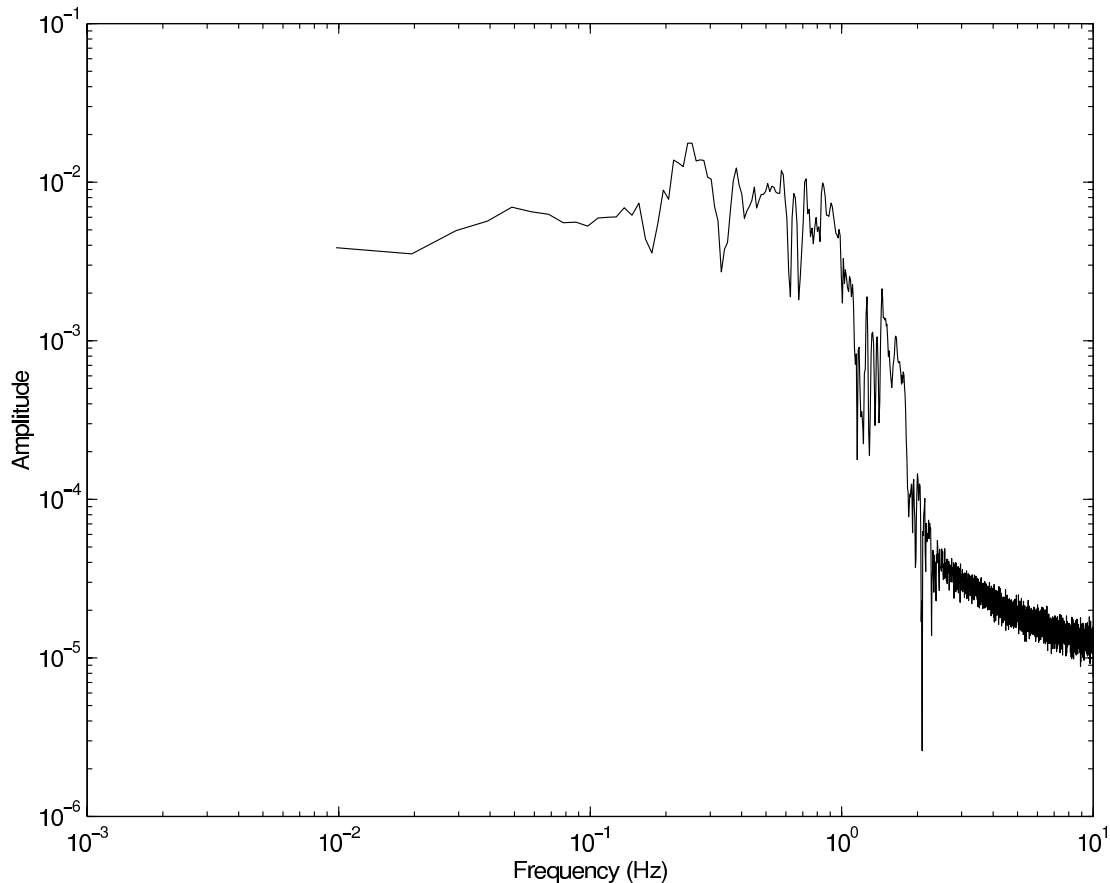
Figure 6. Amplitude spectrum of the stacked NE radial-component receiver response for station TATO (from Fig. 5) showing the frequency content, which provides a direct observational basis to determine the frequency-band limits for the following inversion.

relatively short (5 months), only selected data from one temporary station (TWB1) have a good enough signal-to-noise ratio to be used for the receiver function study. Broad-band data from the TATO station are available from 1992 onwards, providing more data for the investigation of the azimuthal variations of receiver functions. Fig. 3 shows the distribution of the selected teleseismic events used in this study. Source parameters of the selected events are obtained from the Preliminary Determination of Earthquake (PDE) report of the United States Geological Survey (USGS).

Broad-band data from teleseismic earthquakes recorded in Taiwan are selected based on the following criteria:

(i) epicentral distance between $25° < \Delta < 100°$;
(ii) magnitude greater than 6.5;
(iii) good signal-to-noise ratio on seismograms.

Since receiver functions for near-vertical angles of incidence are simpler than those for larger angles, seismograms from earthquakes at $30° < \Delta < 100°$ are, in general, appropriate for receiver function study. For epicentral distances less than $30°$, seismograms are generally complicated and dominated by high-frequency seismic waves sampling the Earth's structure laterally at depth ranges from 70 to 700 km. Beyond $100°$, the effects of the core–mantle transition zone on seismograms become significant. In this study, those events within epicentral distance $25° < \Delta < 30°$ were also inspected and selected in order to increase the database and to provide a better azimuthal coverage, especially from the newer BATS stations.

Fig. 4(a) shows the three-component seismograms for a deep Fiji Island earthquake (537 km depth) recorded at station TATO. Predominant *P*-wave arrivals on the vertical component and *S* waves on the horizontal components are apparent. Surface waves are not well developed for this deep event. The three-component seismograms are rotated to radial (RAD) and transverse (TRAN) components, according to the backazimuth (Fig. 4a). Receiver functions for TATO station can be determined after the source equalization process as
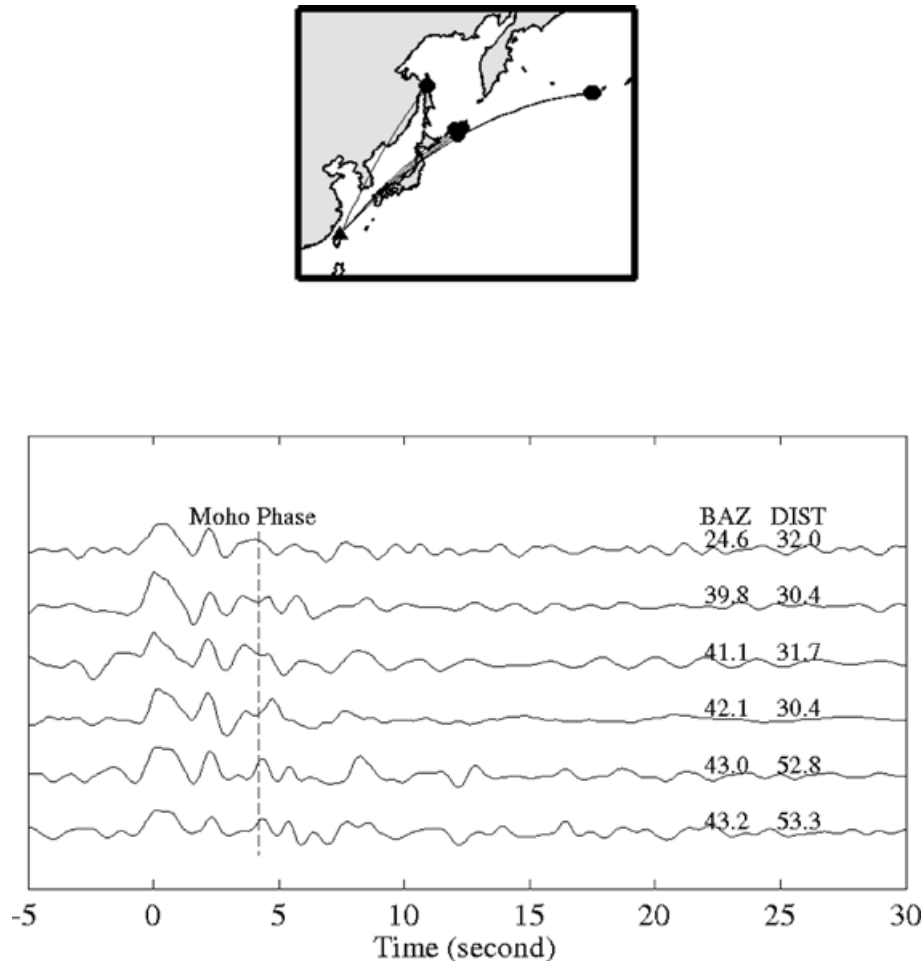
Figure 7. (a) Examples of radial-component receiver functions for TATO station in northern Taiwan using earthquakes from the NE direction. (b) Results of receiver function inversion from the stacked NE receiver functions for TATO station using an initial 1-D model that consists of 1-km layers for the top 10 km and 2-km layers below 10 km. The resultant crustal and upper mantle V_p and V_s structures are shown in the lower figure. The synthetic radial receiver function (thick line) calculated from the inverted velocity structure and the stacked observed radial-component receiver function (thin line) are compared and shown in the top figure. The excellent match between the synthetic and the observed receiver functions as indicated by the high cross-correlation indicator (0.95) suggests that the final V_p and V_s velocity models obtained from the inversion are well determined. The preferred Moho depth is around 30–32 km. (c) Similar to (b), but with a 4-km layer thickness in the initial model. (d) Similar to (b) and (c), but with an 8-km layer thickness in the initial model. (e) Similar to (d), with two layers over a half-space initial model demonstrating that the *P*-to-*S* converted receiver functions form the first (Ps1) and the second (Ps2) layer boundaries as well as the reverberation waves later. (f) Summary of the resultant V_p and V_s structures from (c), (d) and (e), showing that a reliable crustal velocity model can be retrieved with different resolutions, independent of the layer thickness of the initial model.
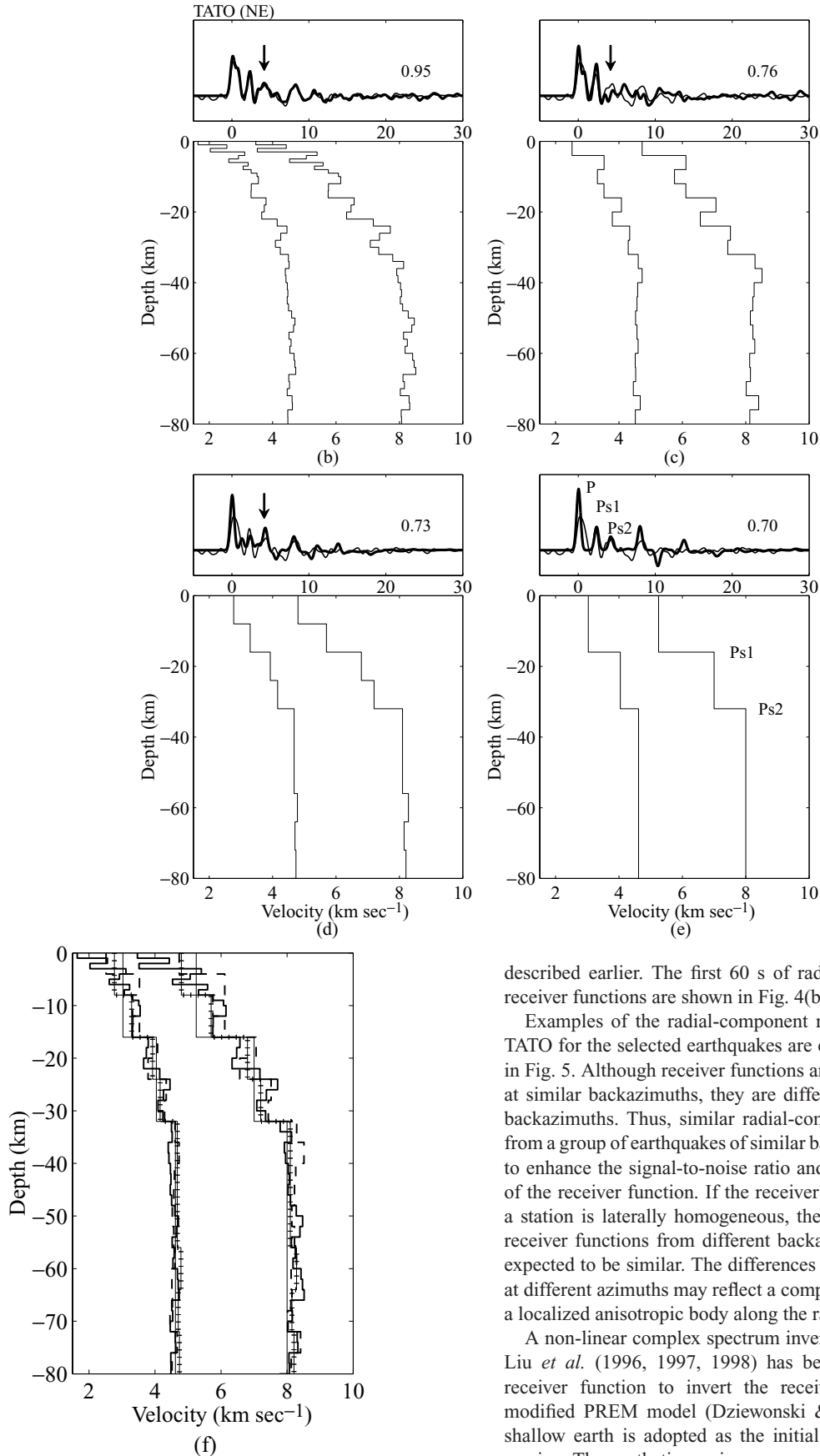
Figure 7. (*Continued.*)

described earlier. The first 60 s of radial (R) and transverse (T) receiver functions are shown in Fig. 4(b).

Examples of the radial-component receiver function at station TATO for the selected earthquakes are calculated and summarized in Fig. 5. Although receiver functions are mostly similar for events at similar backazimuths, they are different for events at different backazimuths. Thus, similar radial-component receiver functions from a group of earthquakes of similar backazimuths can be stacked to enhance the signal-to-noise ratio and to improve the resolution of the receiver function. If the receiver function structure beneath a station is laterally homogeneous, the stacked radial-component receiver functions from different backazimuths at one station are expected to be similar. The differences between receiver functions at different azimuths may reflect a complex subsurface structure or a localized anisotropic body along the ray path.

A non-linear complex spectrum inversion method developed by Liu *et al.* (1996, 1997, 1998) has been applied to the stacked receiver function to invert the receiver function structure. A modified PREM model (Dziewonski & Anderson 1981) for the shallow earth is adopted as the initial velocity model in the inversion. The synthetic receiver response calculated using the given velocity model and the observed receiver response are compared to

determine the variances to evaluate the fitting and the adjustments on the velocity model necessary to improve the fitting during the inversion. The inversion process is iterated, each time with a newly adjusted velocity model. The inversion converges when the adjustments on the velocity model are smaller than a set of given values and the best fit between the observed and the calculated receiver response is reached. The frequency band in the inversion can be determined by the frequency content of a receiver response. The frequency band in this study starts at 0.01–0.5 Hz. After a velocity model from this frequency band is determined, we try to expand the frequency-band upper limit to a higher frequency in order to resolve finer structure. In most cases, the band limit can be expanded to as much as 1.0 or 1.5 Hz. Fig. 6 shows the frequency-domain plot of a receiver function recorded at station TATO, showing that most seismic energy is lower than 1.0 Hz. Throughout the whole iteration procedure, the lower frequency-band limit was fixed at 0.01 Hz.

Because the receiver function analysis deals mainly with the *P*-to-*S* converted phases (P_s) from subsurface discontinuities, and the source equalization process eventually reduces the *P*-type signal and enhances the *S*-type signal, the radial component of the receiver function is very sensitive to the shear-wave velocity structure beneath the receiving station. Therefore, the main result of the inversion process discussed earlier is a representative shear-wave velocity model that produces the best fit between the observed and the calculated receiver functions. The shear-wave velocity structure can be converted to the *P*-wave velocity structure under the assumption of Poisson materials with $V_p/V_s = 1.73$ (e.g. Liu *et al.* 1997). Fig. 7(a) shows examples of radial-component receiver function responses from TATO station for earthquakes from the NE direction. The near-receiver V_s structure can be inverted from the stacked radial-component receiver function using an initial model with 1-km thick layers for the top 10 km, and 2-km thick layers below 10 km (Fig. 7b). The excellent cross-correlation coefficient (0.95) between the observed and the calculated receiver function responses indicates that the inverted V_s and the calculated V_p models are well determined (Fig. 7b). Additional tests of the resolution of inversion of near-receiver structure from the stacked radial-component receiver function were conducted using initial models of various layer thickness. The resultant velocity models and the comparison of the observed and calculated receiver functions using initial models with 4 km and 8 km layer thickness are shown in Figs 7(c) and (d), respectively. The *P*-to-*S* converted arrivals (Ps1 and Ps2) from an oversimplified two layers over a half-space model have been identified in Fig. 7(e). The receiver waveforms after Ps2 can be attributed to the reverberation of *P* and *S* waves inside a two-layer crust. The similarity of the resultant velocity models in Figs 7(b), (c) and (d), as summarized in Fig. 7(f), suggests that major crustal structures can be retrieved regardless of the layer thickness in the initial model, although more structural details and better waveform correlations can be achieved when an initial model with thinner layers is used.

RESULTS

The receiver function method has been used to analyse selected data from 10 broad-band stations (Fig. 2) in order to explore crust and upper mantle structure in Taiwan region. Only eight out of 10 stations have enough good data for a reliable receiver function and velocity structure study. Uncertainties in receiver function responses from the remaining two stations (ANPB and WFSB) in northern Taiwan are large, and these stations will be useful only when additional data become available. In this section, we will discuss crustal struc-
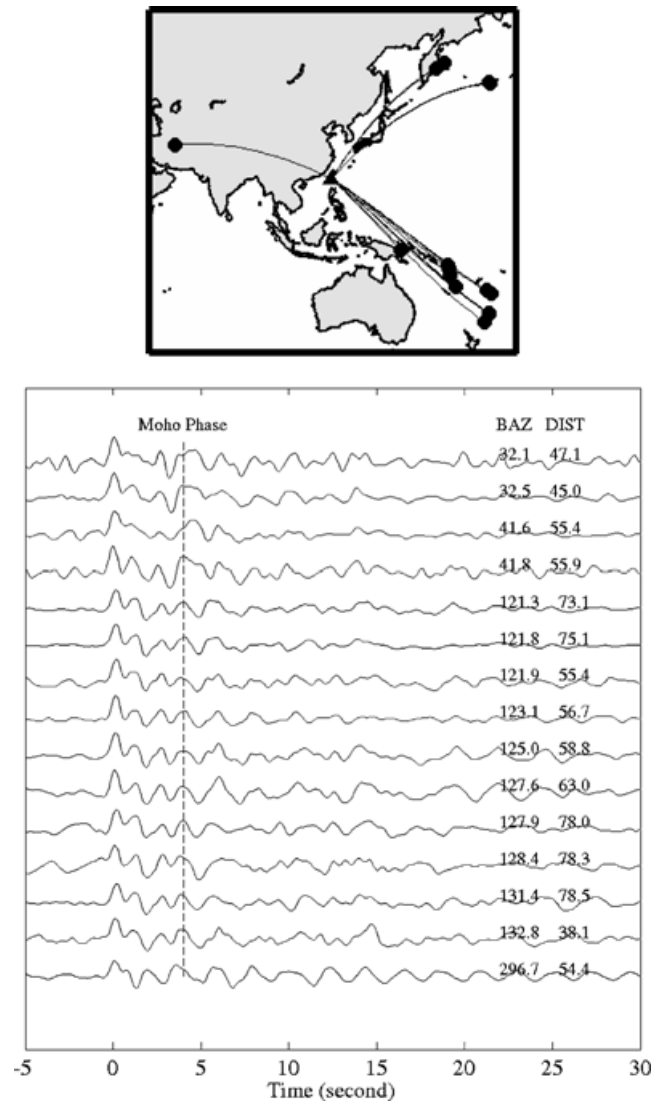
Figure 8. (a) Examples of radial-component receiver functions for TWKB station in southern Taiwan showing very similar receiver function waveforms for earthquakes from all directions. (b) The inversion result for TWKB station is shown with the same format as in Fig. 7. The preferred Moho depth is around 30–32 km.

ture with special focus on the Moho depth from receiver function analysis.

Station TWKB is located at the southern end of Hengchun Peninsula (Fig. 2). The Hegnchun Ridge and portions of the Hengchun Peninsula are the accretionary blocks formed as the South China Sea plate subducted beneath the Philippine Sea plate along the Manila Trench (Chen & Nakamura 1998). Radial-component receiver functions from 15 events recorded at TWKB station are shown in Fig. 8(a). Although there are minor differences between receiver functions from different azimuths, they are sufficiently similar that a representative receiver function can be obtained by a stacking process. Receiver structure for the *S* wave beneath TWKB (Fig. 8b) can thus be inverted from the waveform fitting of the stacked and the calculated receiver functions. The *P*-wave structure is determined by assuming an averaged V_p/V_s of 1.73. The convergence of the receiver function inversion is clearly seen by the excellent match between the observed and the calculated receiver functions. Crustal velocities increase gently as a function of depth. A sharp velocity
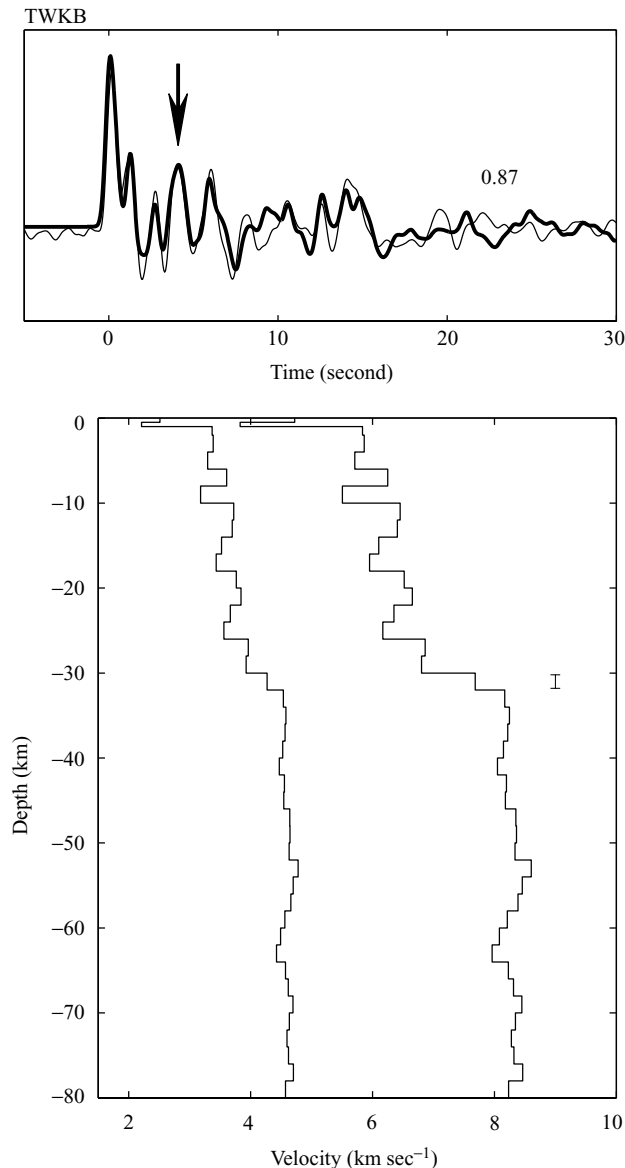
TWKB

0.87

Time (second)

Depth (km)

Velocity (km sec^{-1})

Figure 8. (*Continued.*)

Moho Phase

BAZ DIST
132.0 41.4
130.2 43.9
130.0 44.0

Time (second)

Figure 9. (a) Examples of radial-component receiver functions for TWB1 station in the northeastern corner of Taiwan showing similar receiver function waveforms for earthquakes from the southeast. (b) Inversion results for TWB1 station are shown with the same format as in Fig. 7. The preferred Moho depth is around 20–30 km.

change at a depth of about 30–32 km can be identified with the Moho.

Station TWB1 is located just to the north of the Ilan Plain, at the western terminus of the Okinawa Trough behind the subduction of the Philippine Sea plate along the Ryukyu Trench. The Ilan Plain was formed by a backarc opening along an active volcanic arc (Letouzey & Kimura 1986). Thus the backarc basin overlaps the volcanic arc whose remnants can be found even on the continental side of the basin. However, the Ilan Plain is structurally located on the oceanward side of the Ryukyu arc system. The volcanic ridges in northern Taiwan (Tatun and other volcano groups in northeastern Taiwan) are thus overlapped or are situated behind the backarc basin (Ilan Plain). Waveforms of three events from the SE direction have been used to determine the receiver function for TWB1. As shown in Fig. 9, upper crustal velocities beneath TWB1 seem to be higher than in the lower crust, and the Moho depth is probably around 20–30 km.

Jointly operated by BATS and GSN, TATO station in northern Taiwan has provided more broad-band data for receiver function
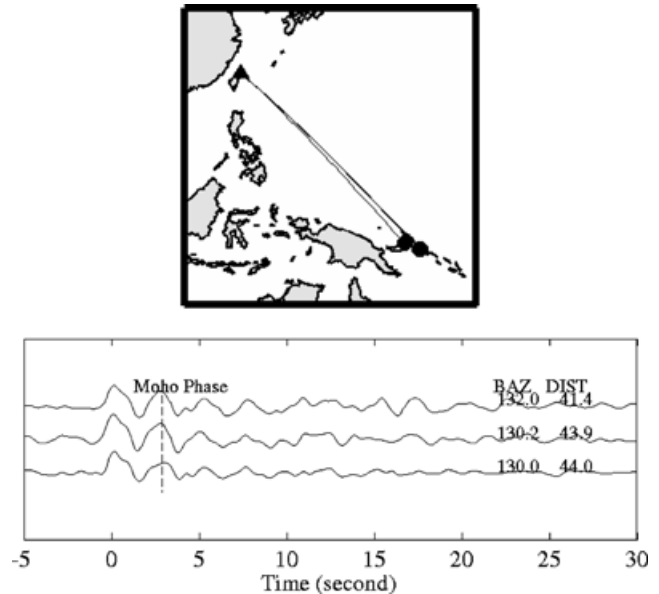
study than any other station in Taiwan. Four events from the SE direction (Fig. 10) and six events from the NE direction (Fig. 7) have been selected for receiver function analysis. Differences in receiver functions between the SE-group and the NE-group (Fig. 4) are apparent. Receiver function structure has been determined for each stacked receiver function. A mid-crust velocity jump at around 18–20 km can be interpreted as the Conrad discontinuity. The Moho depth is estimated to be around 36 km from the SE direction (Fig. 10b) and is about 30–32 km from the NE direction (Fig. 7b), although the velocity transitions in both cases are not very significant. The difference in the Moho depths may be attributable to the sampling of the subduction zone structure from the NE direction but not from the SE direction. The low-velocity lower crust may be related to a region of high geothermal activity associated with the backarc opening.

Station TPUB is located in the Western Foothills, which are composed of Miocene to early Pleistocene shallow and shelf classic sediments that thicken from north to south and from east to west (Ho 1986). The radial-component receiver functions from seven events are shown in Fig. 11(a). A sharp velocity discontinuity separating the upper and lower crust can be clearly identified at a depth of about 20 km, and is probably the Conrad discontinuity. The Moho depth can be identified at about 30–32 km (Fig. 11b).

Station SSLB is located in the Central Mountain Range (Ho 1986). The Central Mountain Range can be subdivided into two parts, namely the Western and the Eastern Central Mountain Ranges. The rocks in the Western Central Mountain Range are coal-bearing and were deposited in a typical continental-shelf environment, while the rocks in the Eastern Central Mountain Range (the Backbone Range) are more finely grained and were deposited close to the continental slope. Thus, it is clear that the Central Mountain Range has been uplifted during the orogenic process. Rapid orogenic process in the Taiwan area is accompanied by a high rate of erosion, and the eroded materials became the source of post-orogenic sedimentary rocks in the Western Taiwan Foothills. Rocks in the Central
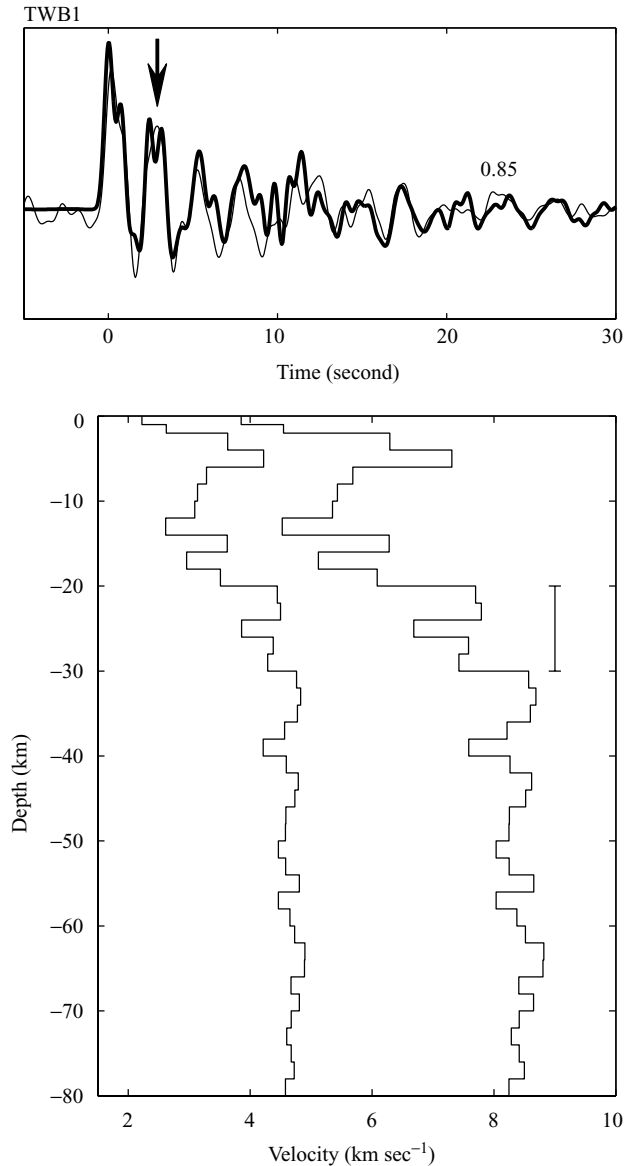
TWB1

Figure 9. (*Continued.*)

Figure 10. (a) Examples of radial-component receiver functions for TATO station showing similar receiver function waveforms for earthquakes from the southeast. (b) Inversion results for TATO-SE are shown with the same format as in Fig. 7. A mid-crust discontinuity can be identified at depth ~20 km which can be interpreted as the Conrad discontinuity. The preferred Moho depth is around 36 km.

Station NACB is located near the northern terminus of a suture zone between the Philippine Sea plate and the Eurasian plate, in other words, close to the most active and advanced collision area in Taiwan (Fig. 1). The erratic crustal velocities shown in Fig. 14 suggest that the crustal structure associated with the collision between the two plates is very complicated. The depth of the Moho is probably around 50–52 km (Fig. 14), which is probably the deepest in this study.

Station KMNB is located on the Eurasian plate close to the coastal region of mainland China. Four events were selected for receiver function analysis. In comparison with results from all the other stations, the crustal velocity structure beneath KMNB station is very simple, representing a typical stable and old continental crust. The depth of the Moho can be easily identified at about 28–30 km (Fig. 15).

Mountain Range have been highly metamorphosed during collision and orogenic processes. The widely distributed thermal hot springs in the Central Mountain Range confirm the observation of high heat flow in the area. Furthermore, an offset of gravity anomaly low from the highest mountain in the Central Mountain Range may imply that the mountain building process is so young that this region has not yet achieved isostatic equilibrium (Yen *et al.* 1998). Crustal velocity is in general higher than at stations TPUB and TATO in the Western Foothills, and seems to increase as a function of depth at a constant rate. The Moho depth can be identified at around 44–46 km, which is much deeper than that associated with stations in the Western Foothills (Fig. 12).

Station TDCB is located in the Western Central Mountain Range. Seven events have been selected for this study. Similar to the results for SSLB, the crustal velocity seems to increase as a function of depth at a constant rate. No dramatic velocity change is apparent in the mid-crust. The Moho transition is not very sharp, but can be estimated to lie in the depth range 40–50 km (Fig. 13).
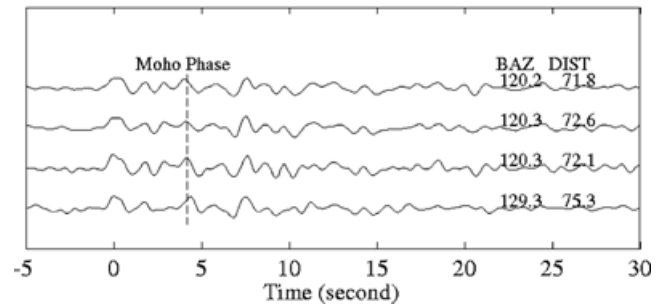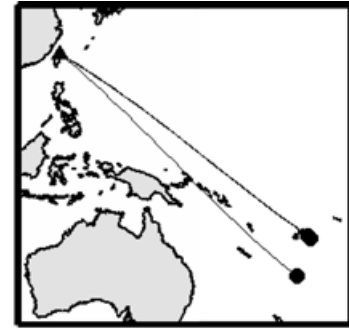
DISCUSSION

Broad-band seismic network monitoring in Taiwan region (BATS) only started in 1994. The installation of BATS is still in progress. Since Taiwan is surrounded by ocean, background noises from the surrounding oceans have been very significant for all broad-band stations. Therefore, with the exception of TATO station, only a very limited amount of high-quality broad-band data from BATS and from a short deployment of 10 PASSCAL broad-band stations in 1995 are available for the receiver function study. Receiver responses beneath Taiwan broad-band stations are, in general, very complex on both the radial and transverse components. It can be inferred from the tectonic history and the complicated receiver response that crustal structure in Taiwan region is characterized by very significant lateral variations. Thus, azimuthal variations of receiver function structures are expected beneath most stations. The currently available broad-band data and sparsely
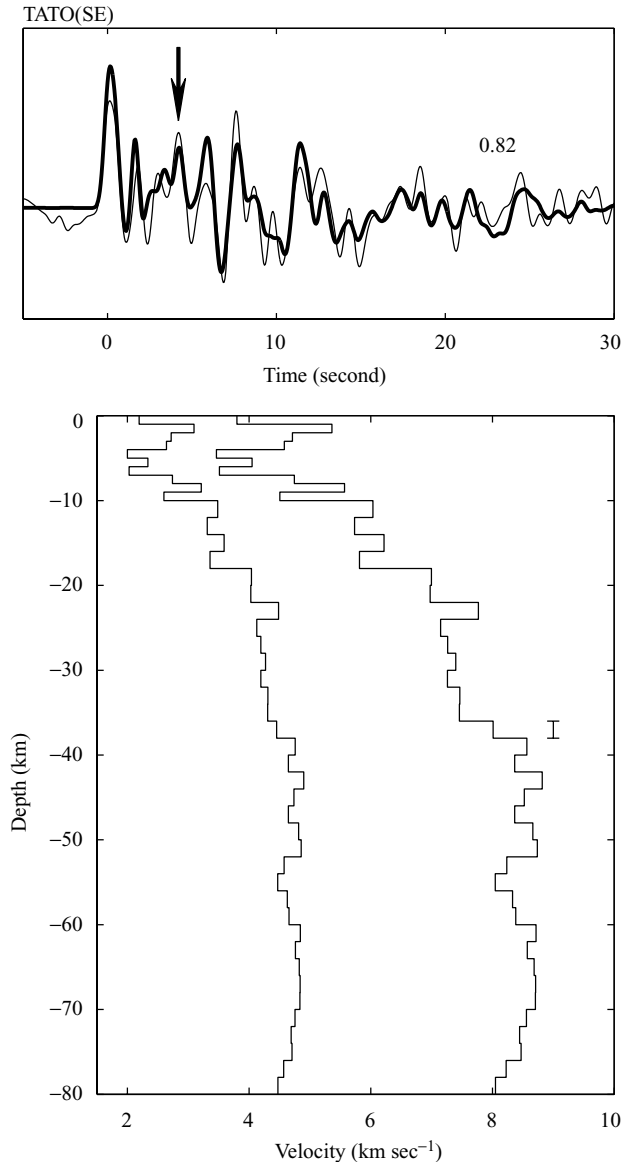
TATO(SE)

Figure 10. (*Continued.*)

Figure 11. (a) Examples of radial-component receiver functions for TPUB station in southwestern Taiwan showing similar receiver function waveforms for earthquakes from the west. (b) Inversion results for TPUB station are shown with the same format as in Fig. 7. A mid-crust discontinuity can be identified at depth ∼20 which can be interpreted as the Conrad discontinuity. The preferred Moho depth is around 30–32 km.

distributed broad-band stations in Taiwan region are not suitable for resolving the complicated effects of subsurface structures from the azimuthal variations of receiver functions. However, prominent subsurface structural features can still be explored based on the results of this study.

The selected 30 s time window beginning from the onset of the P arrival should include seismic energy mainly associated with the direct P and the corresponding converted P_s (S_v type) waves from near-receiver structure. Therefore, the seismic energy related to the direct P and the converted P_s waves should be better observed in the radial component. In this study, we have focused mainly on the analysis of the radial-component receiver function to determine crustal and upper mantle structure. However, we have also investigated the transverse-component receiver function by deconvolving the vertical-component seismogram from the transverse-component seismogram. Fig. 16 shows examples of transverse-component receiver functions from a group of selected data recorded at TATO station. It is immediately obvious that there are very significant seismic arrivals after the first P-wave arrivals on most transverse-
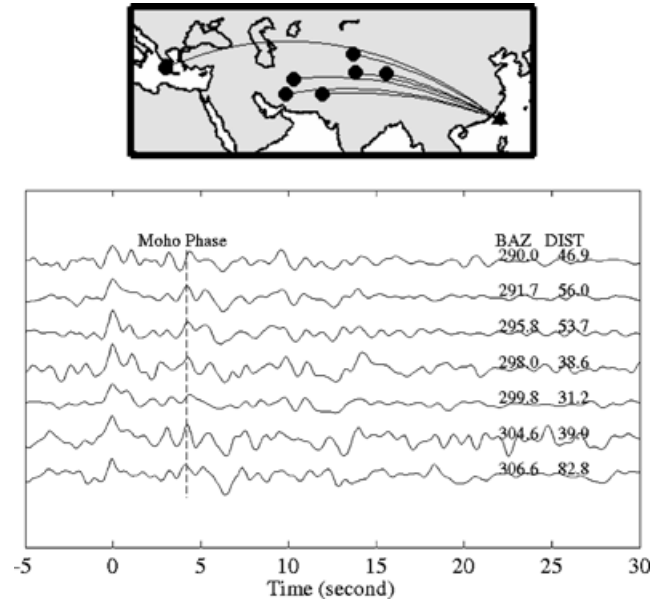
component receiver functions, which is not what we would expect. In some cases, the amplitude of the transverse receiver function may reach one-third to one-half that of the radial component. Many previous studies (e.g. Zhang & Langston 1995; Peng & Humphreys 1997; Chen & Liu 1999) have associated these arrivals on the transverse receiver functions with off-azimuth arrivals, or noises, or dipping interfaces, or an anisotropic body, or anomalous scattering, or event mislocation, or malfunction of instruments, or incorrect sensor orientation, etc. A detailed analysis of transverse-component receiver functions using data from Taiwan broad-band stations was not possible at this time because of the limited amount of available data and the sparse distribution of broad-band stations. This problem can clearly be addressed only if a relatively dense broad-band seismic array can be deployed for a long period in various regions of Taiwan.

Since TATO station has the longest period of operation and thus more data for analysis, significant azimuthal variation of receiver function structure can be clearly seen from the NE and SE directions (Figs 7 and 10). Fig. 17 shows an example of 15-s transverse- and radial-component receiver functions at TATO after the first P onset for events from the NE and SE directions, respectively. The arrival times of the converted P_s phase from the Moho between the NE and SE directions are different, as marked by arrows on the two radial components, and the observed relatively large seismic energy on the two transverse components may be attributed to the effect of dipping subsurface structure. If dipping structure were the major contributor to the generation of seismic energy on the transverse component, the P_s converted phases would be expected to arrive in phase on the radial and transverse components (e.g. Peng & Humphreys 1997; McNamara & Owens 1993). It is, however, clear that the P_s arrivals are in phase in the SE group (BAZ ≃ 130°), but not in the NE group (BAZ ≃ 40°). Therefore, the converted wave along the NE direction must, after conversion, have travelled through an anisotropic region that is not present on the ray path
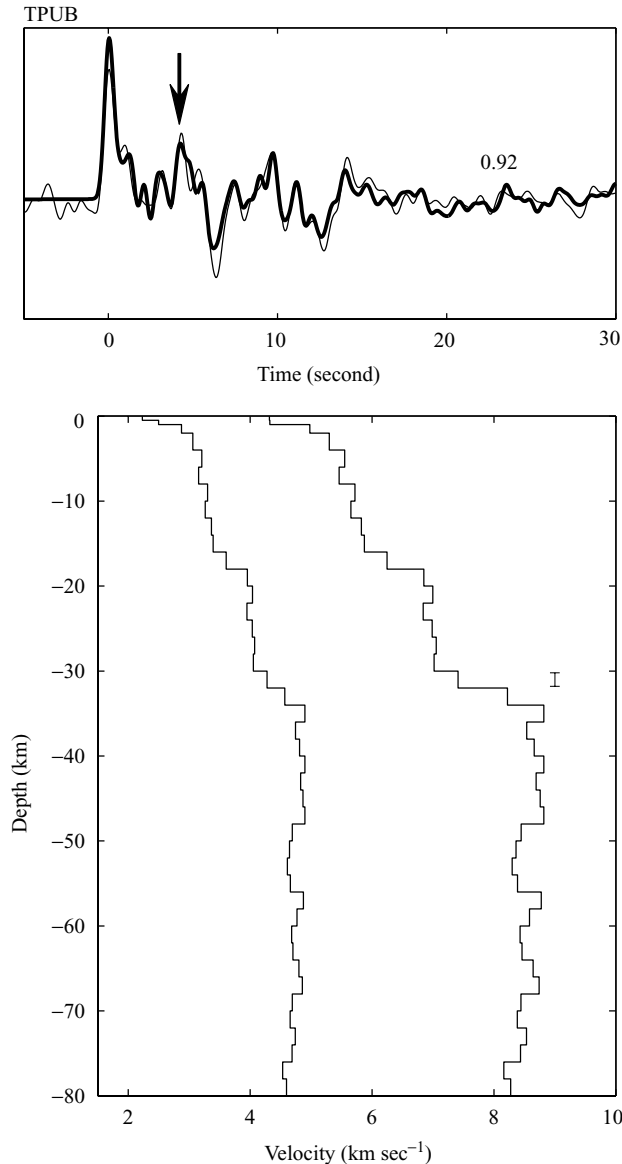
Figure 11. (*Continued.*)

for the SE group. Thus, the above observations at TATO strongly suggest that a dipping subsurface interface and anisotropic region should be considered for crustal structure study in the northern Taiwan region if sufficient high-quality data become available in the future.

Geographically, stations TATO, ANPB, WFSB and TWB1 are very close to each other (Fig. 2), but their receiver functions are quite different, which may point to a significant lateral variation of crustal structure in the northern Taiwan region. Correlation of crustal structure beneath these stations may provide a good opportunity for the study of dipping structure, an anisotropic region or body, and characteristics of the uppermost layer. Several methods have been proposed to study complex crustal structure, including the polarity change of the first *P* arrival in the transverse component (Langston 1977; Liu & Kind 1986; Owens & Crosson 1988; Cassidy 1992; Zhang & Langston 1995; Chen & Liu 1999), the polarity change of the P_s converted phase in the transverse component (Regnier 1988; Zhang & Langston 1995; Peng & Humphreys 1997; Chen & Liu 1999), the delay of the onset time of the first
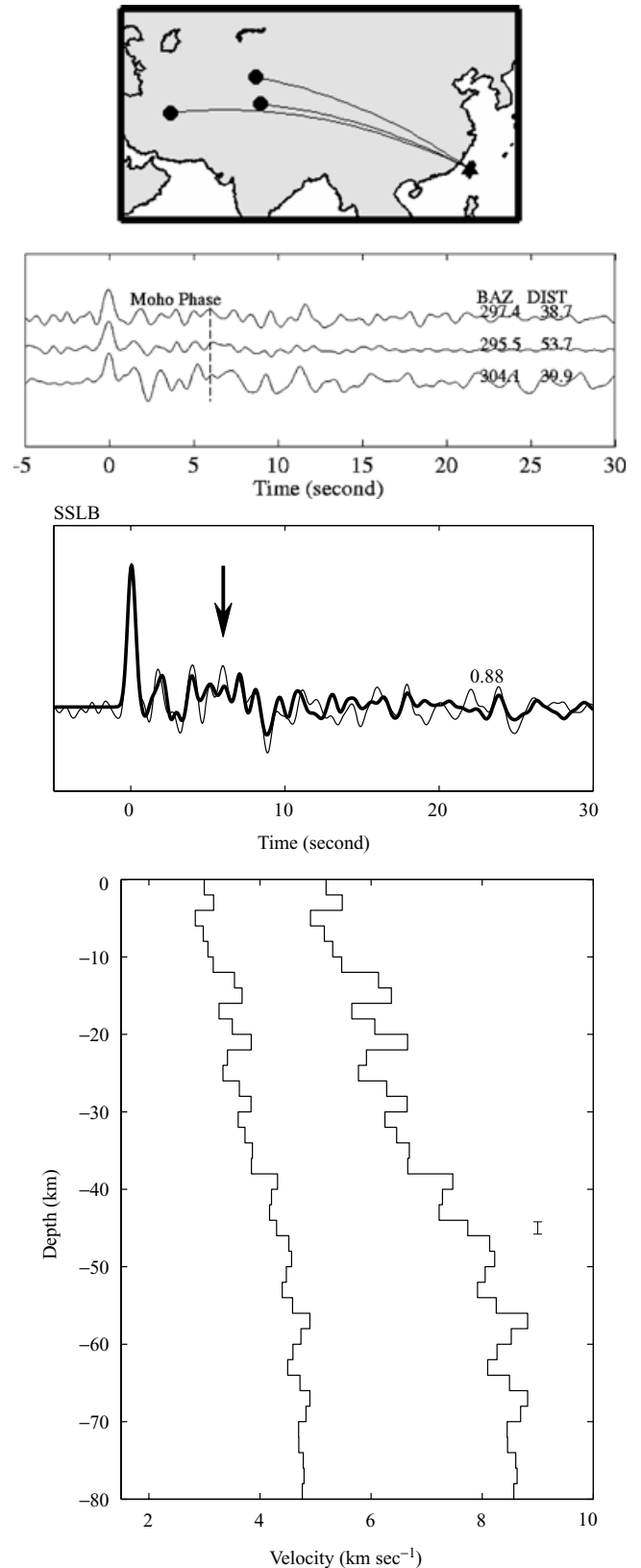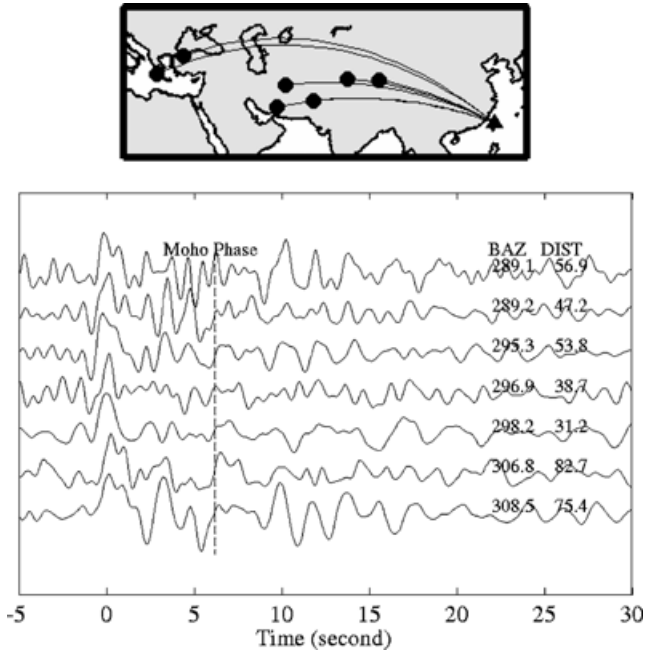

Figure 12. (a) Examples of radial-component receiver functions for SSLB station in the Central Mountain Range showing similar receiver function waveforms for earthquakes from the western direction. (b) Inversion results for SSLB station are shown with the same format as in Fig. 7. Crustal velocities increase steadily as a function of depth from the surface to the bottom of the crust. The preferred Moho depth is around 44–46 km.

Figure 13. (a) Examples of radial-component receiver functions for TDCB station in the Eastern Central Mountain Range showing similar receiver function waveforms for earthquakes from the west. (b) Inversion results for TDCB station are shown with the same format as in Fig. 7. Similar to the SSLB station, crustal velocities increase steadily as a function of depth from the surface to the bottom of the crust. The preferred Moho depth is within the range 40–50 km.

P arrival in the radial component (Owens & Crosson 1988; Mangino *et al.* 1999), the time difference between P and P_s on the receiver response (Regnier 1988; Regnier *et al.* 1994), the identification of arrival energy type by the product of vertical component and radial component after rotation of the seismogram (Jacob & Booth 1977; Kanasewich 1981; Regnier *et al.* 1994), and the arrival time of the *PpPmp* phase shown on the vertical-component seismogram (Baker *et al.* 1996). All of the above-mentioned methods could be applied to study the complex structure in Taiwan region if high-resolution broad-band data and denser station coverage become available in the future.

Radial-component receiver functions for ANPB station can be sorted into NE, SE, and W groups from their backazimuths (Fig. 18a). Radial-component receiver functions are similar within each group and are different between groups. Therefore, similar receiver functions within each group can be stacked to enhance the signal-to-noise ratio as shown in Fig. 18(b). The stacked receiver functions show a different offset time from that of the vertical component (the zero reference time is marked by the vertical line), which may be related to a subsurface dipping layer at shallow depth (Mangino *et al.* 1999). However, more data will be needed for further detailed study of the dipping layer.

In general, the crustal velocity structure beneath stations TATO and TPUB in the Western Foothills is characterized by a mid-crust discontinuity, interpreted as the Conrad discontinuity, at a depth of 18–20 km which is absent beneath stations SSLB and TDCB in the Central Mountain Range. The steady increase of crustal velocity at an almost constant rate from the near surface to lower crust beneath SSLB and TDCB stations suggests that there are no major lithological transitions across the entire thickness of the crust, and probably the evolution process of the thicker crust underneath
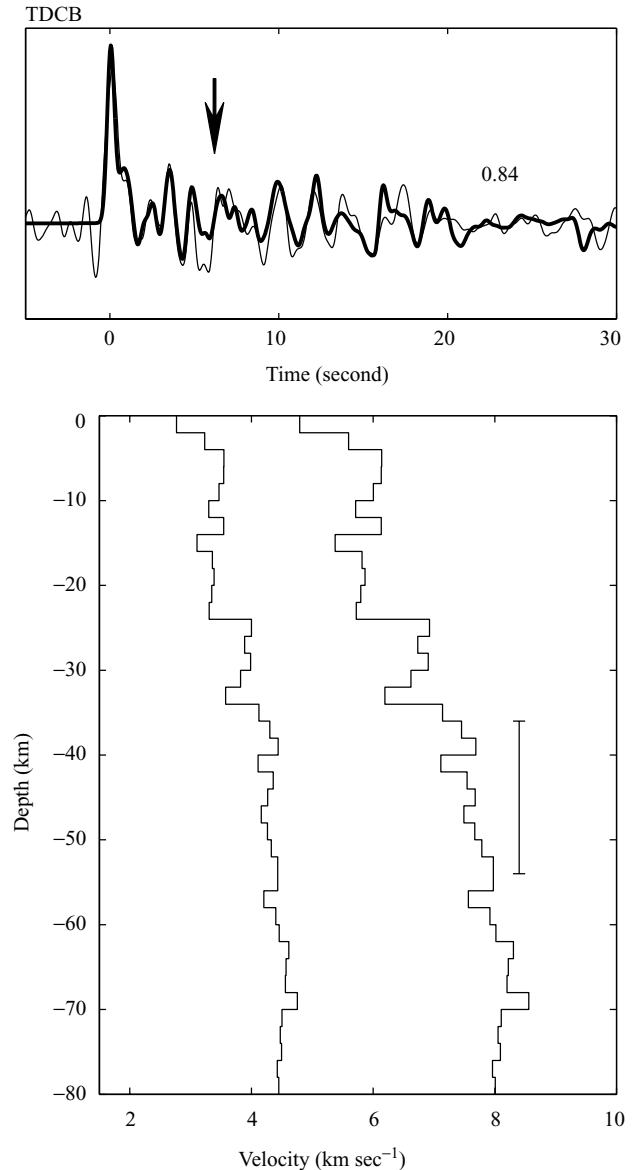
Figure 13. (*Continued.*)

the Central Mountain Range is not the same as that beneath the Western Foothills. Therefore, the contrast in crustal velocity structure and crust thickness between the Western Foothills and Central Mountain Range may imply a major difference in the tectonic models applicable to the region. For example, the 'thin-skinned' deformation model (e.g. Suppe 1976, 1980, 1981, 1984, 1987) probably can explain the tectonic evolution of the upper crust of the Western Foothills and Coastal Plain, while the 'thick-skinned' model (e.g. Wu *et al.* 1997) probably works better for the Central Mountain Range.

The deepest Moho depth in this study has been identified beneath station NACB (50–52 km) at the northern end of the Longitudinal Valley where the most advanced collision between the Eurasian and Philippine Sea plates took place. Thus, there is a very high possibility that the thickest crust in Taiwan region may be offset to the east of the topographic high in the Eastern Central Mountain Range. This observation is supported by the results of a recent modelling of high-resolution gravity data (Yen *et al.* 1998). The Moho depths beneath other stations decrease from east to west, for example
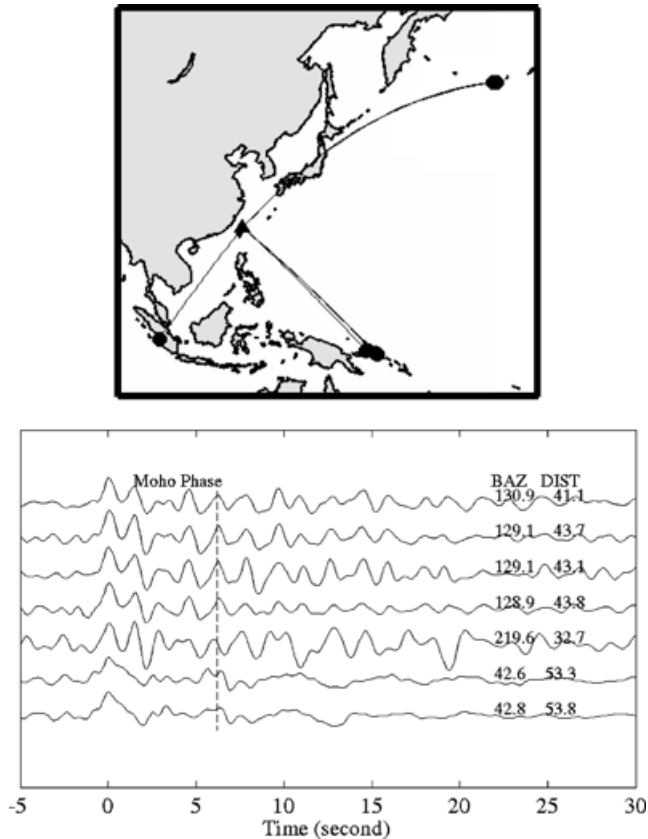
Figure 14. (a) Examples of radial-component receiver functions for NACB station north of the suture zone between the Philippine Sea and the Eurasian plates showing similar receiver function waveforms for earthquakes from all directions except the northeast direction. (b) Inversion results for NACB station are shown with the same format as in Fig. 7. The preferred Moho depth is around 50–52 km.

44–46 km beneath SSLB in the Central Mountain Range, 30–32 km beneath TPUB in the Western Foothills, and 28–32 km at station KMNB, which is a typical thickness for typical continental crust (e.g. Liu *et al.* 1998). The crust is relatively thin (20–30 km) beneath TWB1 station north of Ilan Plain, which could be related to the western terminus of Okinawa trough, a backarc opening behind the Ryukyu trench, which is characterized by high heat flow and thinner crust.

Further crustal structure information can be obtained from an on-shore/offshore wide-angle deep seismic profiling experiment around Taiwan using airgun sources carried out in August and September 1995. Preliminary results from three cross-island seismic profiles (Fig. 2) from this experiment (e.g. Yeh *et al.* 1998; Shih *et al.* 1998; Chen & Nakamura 1998) provide some critical crustal structure information to compare with the results of this study. Preliminary cross-sectional views of crustal structure along lines L1 and L2 are shown in Fig. 19, revealing a general trend of an abrupt thickening of crust from the Philippine Sea plate into the suture zone of eastern Taiwan (from 10–20 km to 45–50 km) and a gradually westward thinning of crustal thickness (about 30 km to the western coastal plain). These results are in good agreement with the variations of crustal thickness obtained from the nearby broad-band stations in this study, for example SSLB, NACB and TDCB near L1, TPUB near L2, and TWKB near L3. Results from TATO and TWB1 are projected to L1 and TWKB is projected to L2 for purposes of comparison, although they are far away from the two lines.
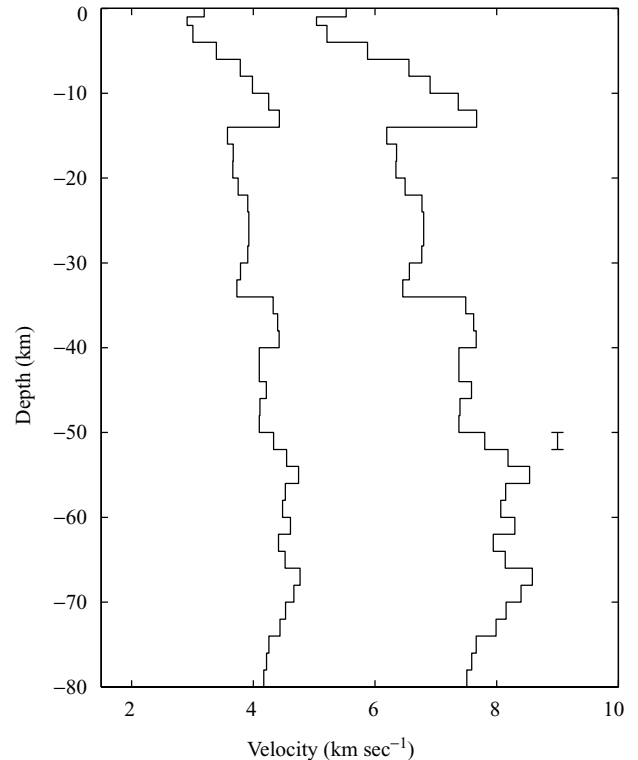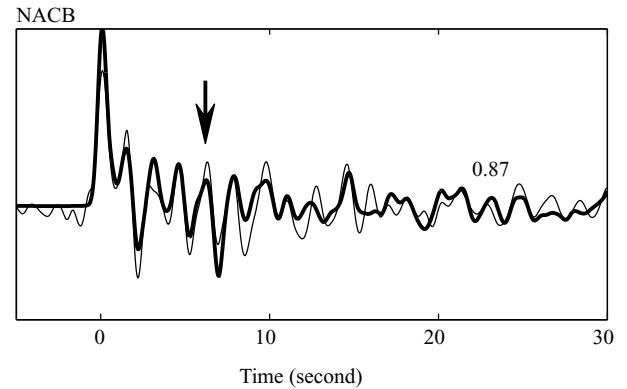
Figure 14. (*Continued.*)

The crustal structure beneath KMNB is relatively simple in comparison with that beneath all the other broad-band stations in Taiwan. A crustal thickness of 28–32 km beneath KMNB is consistent with results from Yuan *et al.* (1986) and Mooney *et al.* (1998) describing a typical old and stable continental crust. The contrast between the simple crustal structure beneath KMNB and the very different and complex crustal structure beneath all other broad-band stations in Taiwan can be attributed to major tectonic differences between a typical stable continent and a young and active subduction and collision-plate boundary.

CONCLUSIONS

The crustal and upper mantle structure beneath 10 selected broad-band stations in Taiwan region has been studied using the receiver function method. The crustal thickness identified from receiver function structure varies from 20–30 km (TWB1) at the backarc opening behind the subduction to about 50–52 km (NACB)
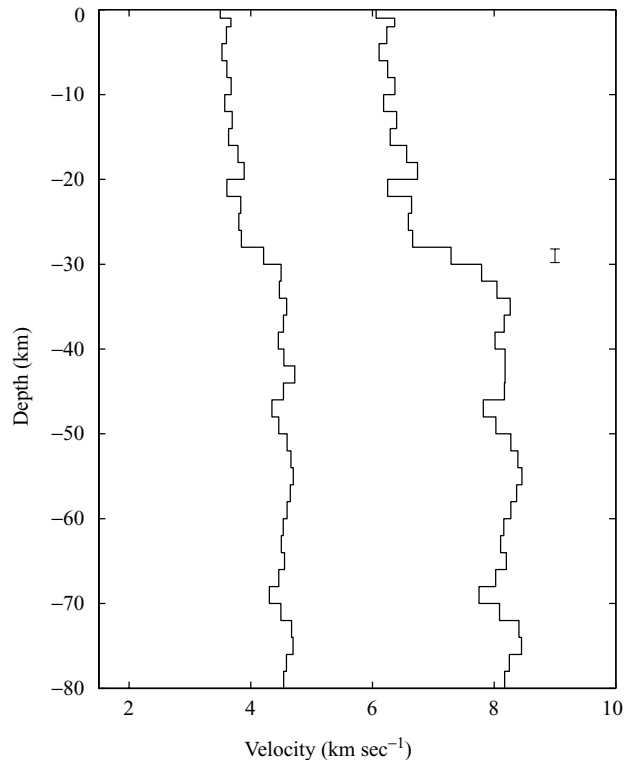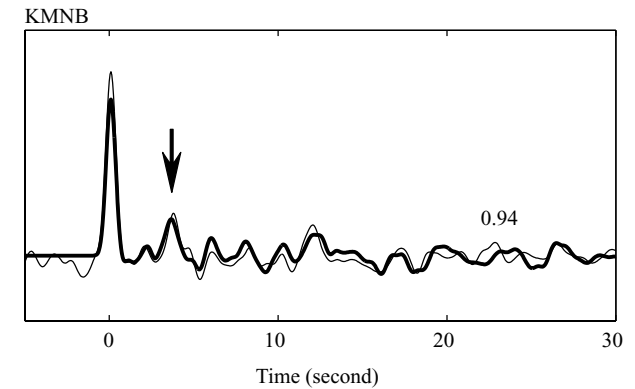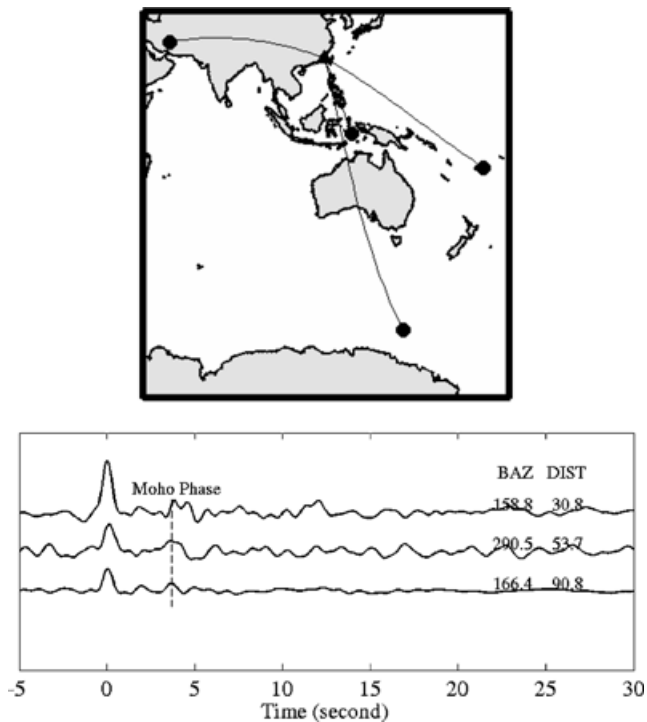
Figure 15. (a) Examples of radial-component receiver functions for KMNB station offshore near the southwestern China mainland showing similar receiver function waveforms for earthquakes from all three directions. (b) Inversion results for KMNB station are shown with the same format as in Fig. 7. The preferred Moho depth is around 28–32 km. Crustal velocity structure beneath the KMNB station is typical for a stable continent and is much simpler than that at all other broad-band stations in Taiwan.

adjacent to the suture zone of active collision between the Philippine Sea and Eurasian plates. The Moho depth decreases from east to west, i.e. 50–52 km at NACB near the collisional boundary in the northern Longitudinal Valley, 44–46 km beneath SSLB in the Central Range, 30–32 km beneath TPUB in the Western Foothills, and 28–32 km beneath KMNB near the China coast. Lateral variations of crustal thickness are consistent with recent results from wide-angle deep seismic profiles (Yeh *et al.* 1998; Shih *et al.* 1998). Crustal velocity structures are very complicated and differ significantly beneath all selected broad-band stations in Taiwan region, a fact which can be associated with the very young, active, and complex tectonics processes resulting in very significant lateral structural variations. However, the crustal velocity structure beneath KMNB near China is very simple and represents a typical old and stable continental crust.

The difference in crustal thickness and the patterns of crustal velocity variations as a function of depth, and the apparent mid-crust discontinuity for stations in the Western Foothills but not for those nearby stations in the Central Mountain Range indicate that the tectonic origin of crust in the two regions may be different. For instance, the 'thin-skinned' deformation model (e.g. Suppe 1976, 1980, 1981) can explain most of the crustal deformation and tectonic evolution in the Western Foothills and Western Coastal Plain, but the 'thick-skinned' or 'lithospheric deformation' model (Wu *et al.* 1997) is probably needed to explain the observations in the Central Mountain Range.

Azimuthal variation of receiver functions can be clearly seen beneath TATO station from the stacking of radial receiver functions for events from the NE and SE directions. Receiver responses from
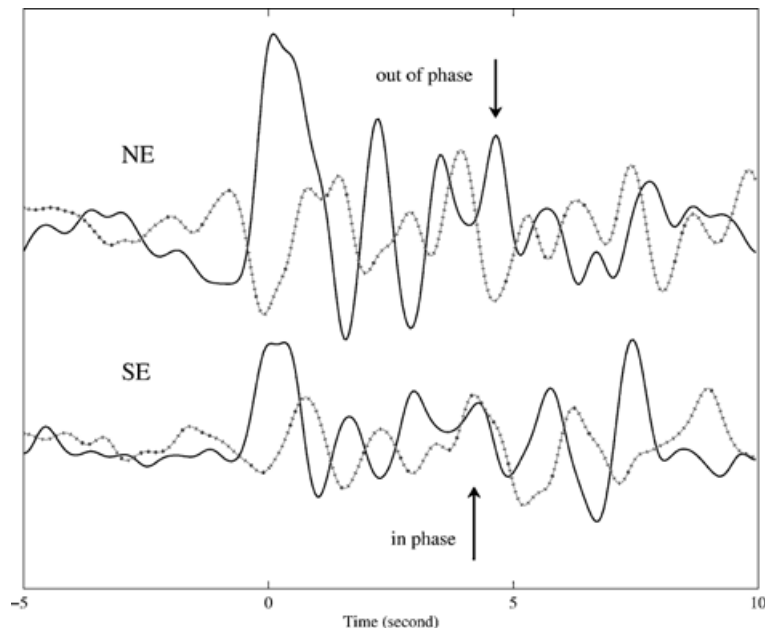

Figure 15. (*Continued.*)

four adjacent stations (TATO, TWB1, ANPB, and WFSB) in northern Taiwan are very different from each other, a fact that could be associated with the effects of complex subsurface structures, for example dipping Moho configuration or subduction zones. A localized anisotropic body in the crust may exist beneath TATO station along the NE direction. Although the currently available broad-band data and the sparse distribution of broad-band stations in Taiwan region prohibit a comprehensive image of crustal structure using the receiver function method, the observed azimuthal variation of receiver functions at TATO and ANPB stations has pointed to the potential of using the receiver function method to study the very complicated subsurface structures, including a dipping interface and anisotropic region, if a denser coverage of broad-band stations can be deployed to collect information from teleseismic events from all azimuths.
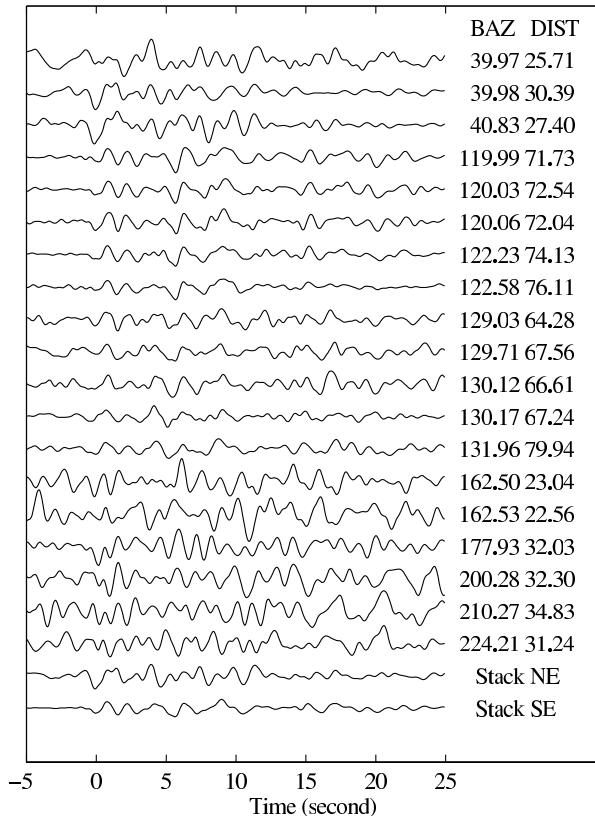
Figure 16. Examples of transverse-component receiver functions recorded at TATO station. Tangential receiver functions for the first three events from similar azimuths are stacked to form a representative receiver function (the second trace from the bottom up, Stacked NE). The next 10 traces at back-azimuths ranging from 119.99° to 131.96° are stacked to form another representative receiver function from the SE direction, as shown in the last trace.

REFERENCES

Ammon, C.J., 1991. The isolation of receiver effects from teleseismic P waveforms, *Bull. seism. Soc. Am.,* **81,** 2504–2510.

Ammon, C.J., Randall, G.E. & Zandt, G., 1990. On the nonuniqueness of receiver function inversions, *J. geophys. Res.,* **95**(B10), 15 303–15 318.

Baker, G.E., Minster, J.B., Zandt, G. & Gurrola, H., 1996. Constraints on crustal structure and complex Moho topography beneath Piñon Flat, California, from teleseismic receiver function, *Bull. Seism. Soc. Am.,* **86,** 1830–1844.

Burdick, L.J. & Langston, C.A., 1977. Modeling crustal structure through the use of converted phases in teleseismic body-wave forms, *Bull. seism. Soc. Am.,* **67,** 677–691.

Cassidy, J.F., 1992. Numerical experiments in broad-band receiver function analysis, *Bull. seism. Soc. Am.,* **82,** 1453–1474.

Chen, J.H. & Liu, Q.Y., 1999. Lithospheric receiver function in 3-D laterally inhomogeneous media using Maslov asymptotic theory, *Acta Geophysica Sinica,* **42,** 84–93.

Chen, A.T. & Nakamura, Y., 1998. Velocity structure beneath the eastern offshore region of southern Taiwan based on OBS data, *TAO,* **9,** 409–424.

Chen, C.S., Chen, C.C. & Chou, K., 1998. Deep electrical structure of Taiwan as inferred from magnetotelluric observations, *TAO,* **9,** 51–68.

Clayton, R.W. & Wiggins, R.A., 1976. Source shape estimation and deconvolution of teleseismic body waves, *Geophys. J. R. astr. Soc.,* **47,** 151–177.

Dziewonski, A.M. & Anderson, D.L., 1981. Preliminary Reference Earth Model, *Phys. Earth planet. Inter.,* **25,** 297–356.

Ho, C.S., 1986. A synthesis of the geologic evolution of Taiwan, *Tectonophysics,* **125,** 1–16.
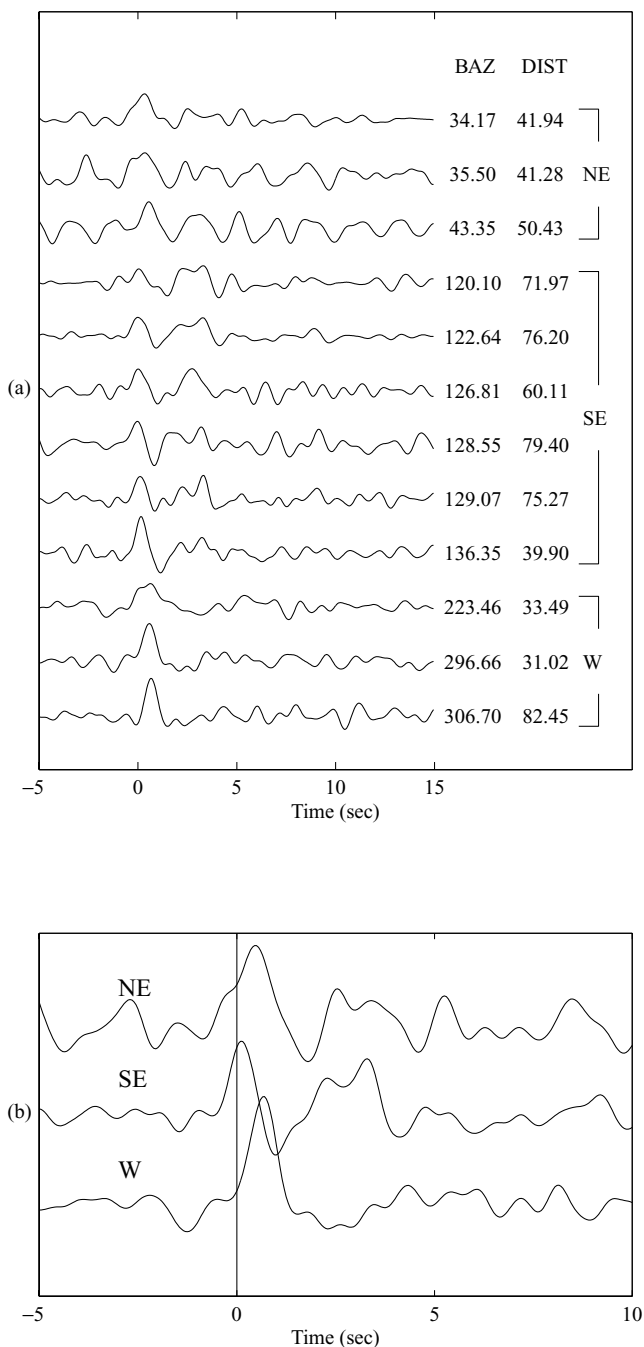

Figure 17. Displays of the first 15 s of radial (solid line) and transverse (dotted line) receiver functions for the stacked NE and SE directions observed at station TATO. Arrows mark the arrival of the P_s converted phase from the Moho, which is out of phase between the radial and transverse components in the NE direction and is in phase in the SE direction. Thus the converted P_s waves have probably travelled across a very localized anisotropic region in the crust beneath TATO station along the NE direction but not along the SE direction.

Figure 18. (a) Radial-component receiver functions for ANPB station, where receiver functions can be grouped into three groups according to their backazimuths and waveform similarities. (b) Stacked receiver functions for the NE, SE, and W groups show different onset times (although the background is relatively noisy). The onset time delay can be as large as 0.7 s along the W direction, which may suggest a west-dipping structure just beneath the free-surface.

Ho, C.S., 1988. *An Introduction to the Geology of Taiwan: Explanatory Text of the Geologic Map of Taiwan,* 2nd edn, p. 192, Cent. Geol. Surv., MEOA, R.O.C..

Jacob, A.W.B. & Booth, D.C., 1977. Observation of PS reflections from the Moho, *J. Geophys., 43,* 687–692.

Kanasewich, E.R., 1981. *Time Sequence Analysis in Geophysics,* University of Alberta Press.

Langston, C.A., 1977. The effect of planar dipping structure on source and receiver responses for constant ray parameters, *Bull. seism. Soc. Am., 67,* 1029–1050.

Langston, C.A., 1979. Structure under mount Rainier, Washington, inferred from teleseismic body waves, *J. geophys. Res., 83*(B9), 4749–4762.

Langston, C.A., 1981. Evidence for the subducting lithosphere under southern Vancouver Island and western Oregon from teleseismic P wave conversions, *J. geophys. Res., 86*(B5), 3857–3866.

Letouzey, J. & Kimura, M., 1986. The Okinawa Trough, genesis, structure and evolution of a back-arc basin developed in a continent, *Tectonophysics, 125,* 209–210.

Liu, Q.Y. & Kind, R., 1986. Lateral variation of the structure of the crust-mantle boundary from conversions of teleseismic P waves, *J. Geophys., 60,* 149–156.

Liu, Q.Y., Kind, R. & Li, S.C., 1996. Maximal likelihood estimation and nonlinear inversion of the complex receiver function spectrum ratio, *Acta Geophysica Sinica, 39,* 531–543.

Liu, Q.Y., Li, S.C., Shen, Y. & Chen, J.H., 1997. Portable broad-band seismic array study of the crustal and upper mantle structure beneath the Yanhui Basin and its neighbor region, *Acta Geophysica Sinica, 40,* 763–772.

Liu, Q.Y., Kind, R. & Li, S.C., 1998. Receiver function at the stations of the Chinese digital seismic network (CDSN) and their nonlinear inversion, *Chinese Journal of Geophysics, 40,* 373–385.

Ma, K.F., Wang, J.H. & Zhao, D.P., 1996. Three-dimensional seismic velocity structure of the crust and uppermost mantle beneath Taiwan, *J. Phys. Earth, 44,* 85–105.

McNamara, D.E. & Owens, T.J., 1993. Azimuthal shear wave velocity anisotropy in the Basin and Range province using Moho Ps converted phases, *J. geophys. Res., 98*(B7), 12 003–12 017.

Mangino, S., Priestley, K. & Ebel, J., 1999. The receiver structure beneath the China digital seismograph network stations, *Bull. seism. Soc. Am., 89,* 1053–1076.

Mooney, W.D., Laske, G. & Masters, T.G., 1998. Crust 5.1: a global crust model at $5° \times 5°$, *J. geophys. Res., 103,* 727–747.

Moores, E.M. & Twiss, R.J., 1995. *Tectonics,* W. H. Freeman and Company.

Owens, T.J. & Crosson, R.S., 1988. Shallow structure effects on broad-band teleseismic P waveforms, *Bull. seism. Soc. Am., 78,* 96–108.

Owens, T.J., Zandt, G. & Taylor, S.R., 1984. Seismic evidence for an ancient rift beneath the Cumberland Plateau, Tennessee: a detailed analysis of broad-band teleseismic P waveforms, *J. geophys. Res., 89*(B9), 7783–7795.

Owens, T.J., Taylor, S.R. & Zandt, G., 1987. Crustal structure at regional seismic test network stations determined from inversion of broad-band teleseismic P waveforms, *Bull. seism. Soc. Am., 77,* 631–662.

Peng, X. & Humphreys, E.D., 1997. Moho dip and crustal anisotropy in Northwestern Nevada from teleseismic receiver functions, *Bull. seism. Soc. Am., 87,* 745–754.

Pujol, J., 2000. Comment on 'Laboratory measurements of ultrasonic wave velocities in rocks from the Campi Flegrei volcanic system and their relation to other data', eds Zamora, M., Sartoris, G. & Chelini, W., *J. geophys. Res., 105*(B9), 21 537–21 542.

Rau, R.J. & Wu, F.T., 1995. Tomographic imaging of lithospheric structures under Taiwan, *Earth planet. Sci. Lett., 133,* 517–532.

Regnier, M., 1988. Lateral variation of upper mantle structure beneath New Caledonia determined from *P*-wave receiver function: evidence for a fossil subduction zone, *Geophys. J., 95,* 561–577.

Regnier, M., Chiu, J.M., Smalley, R. Jr, Isacks, B.L. & Araujo, M., 1994. Crustal thickness variation in the Andean Foreland, Argentina, from converted waves, *Bull. seism. Soc. Am., 84,* 1097–1111.

Seno, T., Stein, S. & Gripp, A.E., 1993. A model for the motion of the Philippine Sea plate consistent with NUVEL-1 and geological data, *J. geophys. Res., 98*(B10), 17 941–17 948.

Sercy, C.K., Christensen, D.H. & Zandt, G., 1996. Velocity structure beneath College Station Alaska from receiver functions, *Bull. seism. Soc. Am., 86,* 232–241.

Shih, R.C., Lin, C.H., Lai, H.L., Yeh, Y.H., Hwang, B.S. & Yen, H.Y., 1998. Preliminary crustal structures across central Taiwan from modeling of the onshore-offshore wideangle seismic data, *TAO, 9,* 317–328.
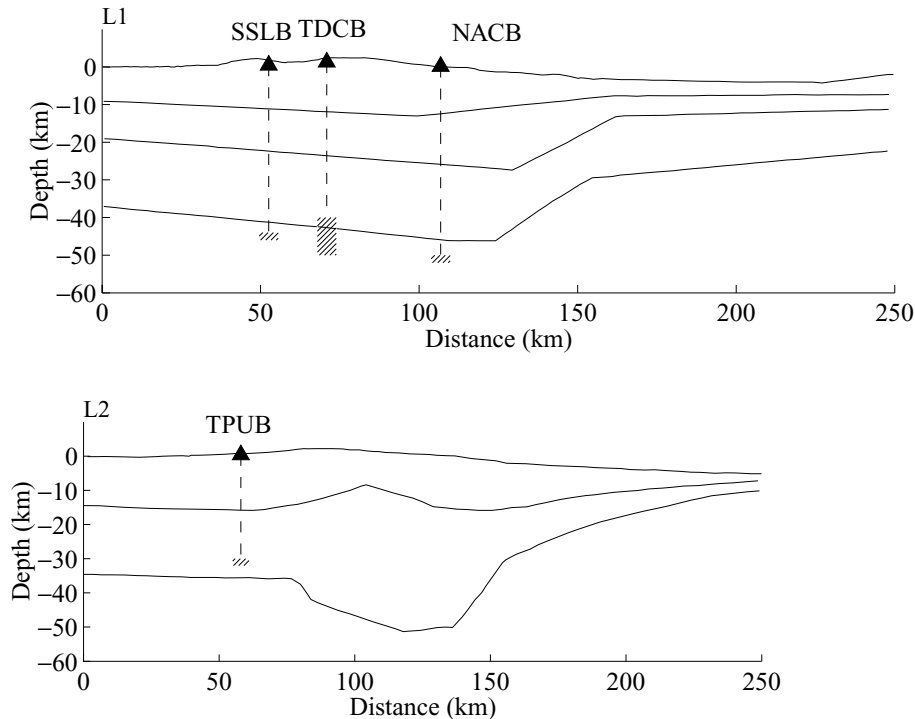
Figure 19. Crustal velocity structure contours duplicated from the preliminary results of onshore/offshore wide-angle deep seismic profiles along the Central Cross-island Highway, L1, from Yeh *et al.* (1998) (top) and along the Southern Cross-island Highway, L2, from Shih *et al.* (1998) (bottom). Stations SSLB, TDCB, and NACB are close to line L1, and the Moho depths obtained in this study beneath these stations are very consistent with that obtained from the seismic line. Station TPUB is very close to line L2, and its Moho depth is consistent with that obtained from the seismic line.

Shumway, R.H. & Der, Z.A., 1985. Deconvoluf multiple time series, *Technometrics,* **27,** 385–393.

Suppe, J., 1976. Decollement folding in western Taiwan, *Pet. Geol. Taiwan,* **13,** 25–35.

Suppe, J., 1980. Imbricate structure of western Foothills belt, south-central Taiwan, *Pet. Geol. Soc. China,* **4,** 67–89.

Suppe, J., 1981. Mechanics of mountain building and metamorphism in Taiwan, *Mem. Geol. Soc. China,* **4,** 67–89.

Suppe, J., 1984. Kinematics of arc-continent collision, flipping of subduction, and back-arc spreading near Taiwan, *Mem. Geol. Soc. China,* **4,** 21–33.

Suppe, J., 1987. The active Taiwan mountain belt, in *The Anatomy of Mountain Ranges,* pp. 277–293, eds Schaer, J.P. & Rodgers, J., Princeton Univ. Press, Princeton, NJ.

Tarantola, A., 1987. *Inversion Problem Theory, Method for Data Fitting and Model Parameter Estimation,* Elsevier, Amsterdam.

Teng, L.S., 1990. Geotectonic evolution of late Cenozoic arc-continental collision in Taiwan, *Tectonophysics,* **183,** 57–76.

Wu, F.T., Rau, R.J. & Salzberg, D., 1997. Taiwan orogeny: thin-skinned or lithospheric collision?, *Tectonophysics,* **274,** 191–220.

Yeh, Y.H. *et al.,* 1998. Onshore/offshore wide-angle deep seismic profiling in Taiwan, *TAO,* **9,** 301–316.

Yen, H.Y., Yeh, Y.H. & Wu, F.T., 1998. Two-dimensional crustal structures of Taiwan from gravity data, *Tectonics,* **17,** 104–111.

Yu, S.B. & Kuo, L.C., 1993. Utilizing continuous GPS data to study the crustal deformation in Taiwan, *Bull. Inst. Earth Sciences, Academia Sinica,* Taipei, Taiwan, R.O.C., **13,** 77–82.

Yu, S.B., Chen, H.Y. & Kuo, L.C., 1997. Velocity field of GPS stations in the Taiwan area, *Tectonophysics,* **274,** 41–59.

Yuan, X., Wang, S., Li, L. & Zhu, J., 1986. A geophysical investigation of the deep structure in China, in *Reflection Seismology: A Global Perspective,* Geodynamic Ser. 13, pp. 151–160, American Geophysical Union, Washington, DC.

Zhang, J. & Langston, C.A., 1995. Dipping structure under Dourbes, Belgium, determined by receiver function modeling and inversion, *Bull. seism. Soc. Am.,* **85,** 254–268.